

Fronts and pulses in a class of reaction-diffusion equations: a geometric singular perturbations approach

Geertje Hek*

January 2000

Abstract

In this paper we prove existence of multiple-front solutions in a class of coupled reaction-diffusion equations with a small parameter. By a travelling wave Ansatz we reduce the problem to a four-dimensional system of ordinary differential equations and prove existence of a large variety of n -jump homoclinic and heteroclinic solutions, $n = 1, 2, 3, \dots$ using geometric singular perturbation theory and Poincaré maps. Numerical simulations of the reaction-diffusion equations indicate that several of the multi-front type waves can be stable.

1 Introduction

In this work we consider the existence problem for travelling ‘localized’ structures in a class of singularly perturbed reaction-diffusion equations. These systems of two reaction-diffusion equations can be reduced to a certain type of four-dimensional flows by a travelling wave Ansatz. The starting point of this research was the study of travelling structures in Ginzburg-Landau (GL) and Nonlinear Schrödinger type of modulation equations. There, a priori, one would also expect a reduction to a four-dimensional system, but owing to a phase invariance one ends up with a three dimensional reduced ordinary differential equation (ODE). In the GL context, existence and bifurcations of homoclinic solutions are extensively studied; see for instance [5] and references there. They are also studied in model problems in [9, 8, 13, 1]. These solutions correspond to an overwhelming richness of travelling localized structures that connect one or two different ‘basic’ patterns. These localized structures may take the form of a front, a pulse, or a multi-front (i.e. a travelling solution with N layers). As the three-dimensional phase space for the travelling wave problem in the GL equation, the model problems contain a one-dimensional slow manifold, possibly with fixed points on it, and a perturbed homoclinic manifold. The studies of these problems made clear that the flow on the slow manifold has an essential influence on the existence of orbits homoclinic to that slow manifold.

In the present work we show, that the methods developed in [9, 8, 13] can also be applied to four-dimensional systems. As in these papers, we use a combination of topological and analytical, asymptotic methods to study existence of homoclinic and heteroclinic

*Mathematical Institute, Utrecht University, P.O. Box 80.010, 3508 TA Utrecht, The Netherlands.
Email:hek@math.uu.nl

solutions. We will again find that the flow on the slow manifolds plays a significant rôle in the existence of homoclinic and heteroclinic solutions. Since the slow manifolds are two-dimensional in this case, the so-called slow flow is less trivial than in the problems in [9, 8, 13] and may allow an even richer structure than the structures found there.

The most general form of the systems we study in the current paper is

$$(1.1) \quad \begin{aligned} U_t &= U_{xx} + F(U, P) + \varepsilon G(U, U_x, P, P_x), \\ \varepsilon^\nu P_t &= P_{xx} + \varepsilon^\mu K(U, U_x, P, P_x). \end{aligned}$$

For $\varepsilon = 0$, $\nu, \mu > 0$, this problem reduces to

$$(1.2) \quad \begin{aligned} U_t &= U_{xx} + F(U, P), \\ P &= P_0, \end{aligned}$$

in the space of bounded, continuous functions. Thus, (1.1) can be interpreted as a ‘standard’ scalar nonlinear diffusion equation, of which the coefficients have become functions that vary slowly in space and time. This variation is then prescribed by the full system (1.1). For $\nu = 0$, $\mu > 0$, the $\varepsilon = 0$ limit is

$$(1.3) \quad \begin{aligned} U_t &= U_{xx} + F(U, P), \\ P_t &= P_{xx}. \end{aligned}$$

The motivation to study these systems is mostly a mathematical one, but of course the diffusion and reaction terms have a physical interpretation in many problems in for instance chemistry and biology. In the form (1.1) the function G is a small ‘convection’ term, it may for instance also contain a chemotactic coupling $\frac{\partial}{\partial x}(U_x H(U, P))$, $H > 0$, between U and P (see for instance [20]). The theory we develop can also be applied in this case, since expansions in the small parameter ε yield a system that is, in essence, of the form (1.7) that we derive here.

From a mathematical point of view we show how geometrical methods, that are developed for singular perturbations of three-dimensional systems possessing a homoclinic manifold, can be applied to four-dimensional systems.

We choose F such that (1.2) possesses two asymptotically stable, stationary states U_- and U_+ for a continuous family of P_0 , so

$$F(U_\pm, P_0) = 0 \text{ and } \frac{\partial}{\partial U} F(U_\pm, P_0) < 0$$

by a linear stability analysis. For simplicity we choose F to be a cubic polynomial in U , satisfying these conditions. In general (1.2) would then permit one front solution, travelling with a unique constant speed $c \neq 0$, connecting U_- with U_+ . For this fixed c this gives the opportunity to jump either from U_- to U_+ in terms of heteroclinic orbits, or from U_+ to U_- . In this paper we want to focus on the case in which orbits can jump back as well, since this may give rise to multi-jump orbits in the perturbed system as described below. We therefore impose that F is symmetric, and we make the explicit choice

$$(1.4) \quad F(U, P) = f(P)(U - U^3),$$

where $f(P) > 0$ for $P \in \mathbf{R}$. Hence $U_- = -1$ and $U_+ = +1$, independent of P_0 . This choice does not influence the essence of our results.

By this choice the resulting ODE we derive has an integrable limit as $\varepsilon \downarrow 0$, which possesses two planes $U = -1$ and $U = +1$ filled with saddle equilibria and two heteroclinic manifolds consisting of families of orbits that connect saddle points on both planes. For $\varepsilon > 0$ but small, the planes $U = \pm 1$ turn into normally hyperbolic slow manifolds, and by a Melnikov method primary heteroclinic orbits that survive the perturbation can be found. These basic, primary heteroclinic orbits form a framework on which more complicated orbits can be built. These orbits consist of fast jumps that follow one of the primary heteroclinic orbits, and trajectories along both slow manifolds that connect the fast jumps to each other. This basic framework is determined by the fast flow, but whether or not the jumps can be connected is very much influenced by the flow on the slow manifolds. In sections 3 and 4 we prove for arbitrary $n > 0$ that, under certain conditions on the parameters, rich classes of such complicated orbits with n jumps through the fast field exist.

The models that are developed and studied in [9, 8, 13, 1] are perturbations of a three-dimensional flow possessing a line of saddle-points and a homoclinic manifold that connects the saddle-equilibria to themselves. In the perturbed systems the axis of saddle points becomes a hyperbolic slow manifold and the occurrence of cascades of homoclinic bifurcations or even explosions of homoclinic orbits to this manifold is proved. These orbits all make their fast loops close to two primary 1-loop homoclinic orbits. For certain systems of the type

$$(1.5) \quad \begin{aligned} \dot{x} &= y, \\ \dot{y} &= x - x^2 + \varepsilon F_1(x, y, z; q), \\ \dot{z} &= \varepsilon F_2(x, y, z; p), \end{aligned}$$

where $\dot{} = \frac{d}{dt}$ and p, q are parameters, existence of a horseshoe and an uncountable set of homoclinic orbits that make as many circuits through the fast field as one wishes are proved in [13]. In the original partial differential equations (PDEs) such orbits correspond to travelling orbits with arbitrarily many pulses. In GL context the primary, 1-loop homoclinic orbits are unstable [12], so multi-circuit homoclinic orbits built on them are likely unstable as well.

Here we however study systems that give rise to families of heteroclinic rather than homoclinic solutions in the unperturbed ($\varepsilon = 0$) case. If multi-jump homoclinic or heteroclinic orbits in the full singularly perturbed problem exist, it follows from the general theory developed in [2] that their spectrum will be close to that of the two primary heteroclinic connections of the scalar equation (1.2). Here ‘close’ means that it will merge with that of the scalar problem in the limit $\varepsilon \rightarrow 0$. Since the two fronts in (1.2) with (1.4) are stable [14], it can be expected that at least some of the multi-jump patterns constructed in this paper will be stable. Indeed, numerical simulations in section 5 of this paper suggest that certain n -front solutions of a PDE of the type (1.1) are stable, or meta-stable.

Remark 1.1 The recent results on the ODE derived from a GL perturbation of the defocusing nonlinear Schrödinger equation in [18] show that heteroclinic connections corresponding to a *stable* ‘dark’ solitary wave can exist as solution to the original PDE. This

stable structure can possibly be used as the ‘building blocks’ with which multi-circuit homoclinic orbits close to the heteroclinic cycle, maybe corresponding to stable solutions to the PDE, can be constructed.

The solutions we consider are either stationary or travelling with a constant speed $\varepsilon^\lambda c$, $\lambda \geq 0$. We therefore start with the travelling wave Ansatz and put $U = u(\xi)$, $P = p(\xi)$ with $\xi = x - \varepsilon^\lambda ct$ to reduce (1.1) to

$$\begin{aligned} u_{\xi\xi} &= f(p)(u^3 - u) - \varepsilon^\lambda cu_\xi - \varepsilon G(u, u_\xi, p, p_\xi), \\ p_{\xi\xi} &= -\varepsilon^\mu K(u, u_\xi, p, p_\xi) - \varepsilon^{\lambda+\nu} cp_\xi. \end{aligned}$$

The function K is supposed to be the term that determines the main character of the slow flow, therefore we set $\mu \leq \nu + \lambda$. With the definitions $u_\xi = v$ and $p_\xi = \varepsilon^{\mu/2} q$ we obtain the following system of ordinary differential equations

$$(1.6) \quad \begin{aligned} u_\xi &= v \\ v_\xi &= f(p)(u^3 - u) - \varepsilon^\lambda cv - \varepsilon g(u, v, p, q) \\ p_\xi &= \varepsilon^{\mu/2} q \\ q_\xi &= -\varepsilon^{\mu/2} k(u, v, p, q) - \varepsilon^{\lambda+\nu} cq, \end{aligned}$$

where the functions g and k are the equivalents of G and K . The $O(\varepsilon^{\mu/2})$ term is the leading order term in the equation for q_ξ .

Finally, we make assumptions on the scaling of the perturbation terms. When $\lambda = 0$ the $\varepsilon = 0$ fast subsystem of (1.6) is either a forced or a damped oscillator, that does not exhibit any heteroclinic connections for $c \neq 0$. However, when $\lambda > 0$ the $\varepsilon = 0$ fast subsystem does exhibit heteroclinic connections between the two steady states $u = -1$ and $u = 1$ for all c . Moreover, if the wave speed is of the same order as other perturbations, in other words if $\lambda = 1$, then the small forcing or damping $\varepsilon^\lambda cv$ can be balanced by other mechanisms. Thus, we choose $\lambda = 1$. Note, that this scaling should be changed if G only contains terms with factors P_x and the lowest order of the perturbation is smaller than $O(\varepsilon)$.

To obtain equal lowest orders of perturbation in all equations, we choose $\mu = 2$ and end up with

$$(1.7) \quad \begin{aligned} u_\xi &= v, \\ v_\xi &= f(p)(u^3 - u) - \varepsilon cv - \varepsilon g(u, v, p, q), \\ p_\xi &= \varepsilon q, \\ q_\xi &= -\varepsilon k(u, v, p, q) - \varepsilon^{1+\nu} cq. \end{aligned}$$

We show that the approach developed in [8] and [13] can be extended and applied to this model problem. In this, we focus on the influence of the extra (fourth) dimension on the methods, since the geometric ideas behind these methods were, a priori, strictly three-dimensional. The global behaviour of the systems (1.7) appears to be very complicated, and difficult to describe in such a general context. Therefore we do not study (1.7) in its full generality, but choose to focus on simple explicit examples. However, since the methods are mainly of a geometrical nature, they can also be applied to the general model, and to other classes of singularly perturbed ODEs.

In the first example the equations for p and q decouple, but even in this very simple case we prove the existence of four families of n -jump homoclinic and heteroclinic orbits for arbitrary $n > 0$. These results are formulated in Theorems 3.2 and 3.8. In the papers [8, 13] it was shown that so-called counteracting effects gave rise to the above mentioned existence of a horseshoe and an uncountable set of homoclinic orbits. Here we find that the fourth dimension immediately implies some counteracting behaviour, independent of the parameters, and yields two sets of $4n-2$ n -jump orbits; see Theorem 3.10. Finally, we show that the second example, in which the equations are no longer decoupled, exhibits even richer counteracting behaviour, and richer classes of homoclinic and heteroclinic orbits.

The paper is organized as follows. We extend the theory developed in [8] and [13] in section 2 and apply it to an example in sections 3 and 4. Section 5 is devoted to some numerical simulations of front-type solutions that correspond to homoclinic and heteroclinic solutions found in sections 3 and 4. The results and relation to other work are discussed in the last section.

2 Global geometry for $\varepsilon = 0$ and $\varepsilon > 0$

The slow limit of (1.7), obtained by letting $\varepsilon \rightarrow 0$ in that system, defines two-dimensional invariant planes $\{u = +1, v = 0\}$, $\{u = -1, v = 0\}$ and $\{u = 0, v = 0\}$. By the assumptions on $F(U, P)$ the first two,

$$\mathcal{M}_{\pm} \stackrel{\text{def}}{=} \{u = \pm 1, v = 0\},$$

are filled with hyperbolic equilibria, and are thus normally hyperbolic. Note that this is a consequence of considering p and $q = \frac{p\xi}{\varepsilon}$ as variables instead of p and $p\xi$. For $\varepsilon = 0$ the system (1.7) has three integrals

$$(2.1) \quad E(u, v, p) = \frac{1}{2}v^2 + \frac{1}{2}f(p)u^2 - \frac{1}{4}f(p)u^4, \quad p \text{ and } q.$$

For each $p, q = \text{const.}$ \mathcal{M}_- and \mathcal{M}_+ are connected to each other by two heteroclinic orbits. The two families of heteroclinic orbits form the compact parts \mathcal{H}_{\pm} of the level set $E(u, v) = \frac{1}{4}f(p)$. They are subsets of the stable and unstable manifolds of \mathcal{M}_{\pm} . Here the convention is that \mathcal{H}_+ contains orbits with $v > 0$ and \mathcal{H}_- contains orbits with $v < 0$. For fixed p, q the two connecting orbits are

$$(2.2) \quad (u_{\pm}(\xi), v_{\pm}(\xi)) = \left(\pm \tanh\left(\frac{1}{2}\sqrt{2f(p)}\xi\right), \pm \frac{1}{2}\sqrt{2f(p)}\left(1 - \tanh^2\left(\frac{1}{2}\sqrt{2f(p)}\xi\right)\right) \right).$$

Inside $\mathcal{H}_+ \cup \mathcal{H}_-$ a family of invariant cylinders filled with periodic orbits exist. The planes \mathcal{M}_{\pm} represent the solutions of (1.1) with trivial U state $U = \pm 1$. Since \mathcal{M}_{\pm} are normally hyperbolic, Fenichel theory [11] guarantees, that any C^2 -small perturbations preserve nearby hyperbolic slow manifolds $\mathcal{M}_{\pm}^{\varepsilon} = \mathcal{M}_{\pm}^c + O(\varepsilon)$ for any compact $\mathcal{M}_{\pm}^c \subset \mathcal{M}_{\pm}$. A special choice of the perturbation $g(u, v, p, q)$ might guarantee that $\mathcal{M}_{\pm}^{\varepsilon} = \mathcal{M}_{\pm}^c$: the manifolds \mathcal{M}_{\pm} are also invariant under the flow of the full, $\varepsilon > 0$, system. This is the case if

$$g(\pm 1, 0, p, q) = 0.$$

We impose this condition on g , since this provides us with exact expressions for $\mathcal{M}_\pm^\varepsilon$ that will be convenient to describe the slow flow in §2.2.

For small $\varepsilon > 0$ the manifolds $\mathcal{M}_\pm^\varepsilon$ no longer consist of fixed points, but are slow manifolds. The slow flow on $\mathcal{M}_\pm^\varepsilon$ is determined by the function $k(u, p)$. We come back to this later. By Fenichel [11] $\mathcal{M}_\pm^\varepsilon$ have stable and unstable manifolds, which we call $\mathcal{W}^s(\mathcal{M}_\pm^\varepsilon)$ and $\mathcal{W}^u(\mathcal{M}_\pm^\varepsilon)$ respectively, that are $O(\varepsilon)$ close to those of $\mathcal{M}_\pm^\varepsilon$. From now on we omit the ε in the notation of \mathcal{M}_\pm and define $W^s(\mathcal{M}_\pm)$ and $W^u(\mathcal{M}_\pm)$ as those parts of $\mathcal{W}^{s,u}(\mathcal{M}_\pm^\varepsilon)$ that merge with $\mathcal{H}_+ \cup \mathcal{H}_-$ as $\varepsilon \rightarrow 0$.

2.1 The fast field: Melnikov calculations

While for $\varepsilon = 0$ $W^u(\mathcal{M}_-) = W^s(\mathcal{M}_+) = \mathcal{H}_+$ and $W^s(\mathcal{M}_-) = W^u(\mathcal{M}_+) = \mathcal{H}_-$, these manifolds can split for $\varepsilon > 0$, giving rise to a splitting distance that is defined more precisely below. However, some intersections $W^u(\mathcal{M}_\pm) \cap W^s(\mathcal{M}_\pm)$ may persist, exactly when this distance is equal to zero. Such intersections consist of solutions $\gamma_h(\xi)$ to (1.7) that lie both on an unstable manifold $W^u(\mathcal{M}_+)$ or $W^u(\mathcal{M}_-)$ and on a stable manifold $W^s(\mathcal{M}_+)$ or $W^s(\mathcal{M}_-)$, and thus approach \mathcal{M}_+ or \mathcal{M}_- for $\xi \rightarrow \pm\infty$. Since $W^s(\mathcal{M}_\pm)$ and $W^u(\mathcal{M}_\pm)$ are three-dimensional manifolds by the assumptions on $F(U, P)$ and by Fenichel [11], $W^s(\mathcal{M}_\pm) \cap W^u(\mathcal{M}_\pm)$ generically is a two-dimensional manifold, if it is non-empty. Equivalently, one expects one or more one-parameter families of orbits γ_h that connect \mathcal{M}_\pm to themselves or to each other. In order to find these homoclinic or heteroclinic solutions, we employ an adiabatic Melnikov method [21, 24] that measures the splitting distance between respectively the manifolds $W^u(\mathcal{M}_-)$ and $W^s(\mathcal{M}_+)$, or $W^u(\mathcal{M}_+)$ and $W^s(\mathcal{M}_-)$. This splitting distance can respectively be measured in the hyperplanes $\Sigma_+ = \{u = 0, v > 0\}$ and $\Sigma_- = \{u = 0, v < 0\}$.

Since the system (1.7) is an $O(\varepsilon)$ perturbation of an integrable system with periodic orbits inside the manifolds \mathcal{H}_\pm , components of $W^u(\mathcal{M}_\pm)$, $W^s(\mathcal{M}_\pm)$ inside \mathcal{H}_\pm will intersect the hyperplane $\{v = 0\}$ many times. Therefore we may expect homoclinic or heteroclinic orbits to \mathcal{M}_\pm that intersect $\{v = 0\}$ more than once. We make a distinction between the *first* intersections $W^u(\mathcal{M}_+) \cap W^s(\mathcal{M}_-)$ or $W^u(\mathcal{M}_-) \cap W^s(\mathcal{M}_+)$, corresponding to the *first* heteroclinic orbits, and next intersections. The first heteroclinic orbits make one jump through the fast field, next orbits make more than one jumps. For convenience we denote the first intersections of $W^u(\mathcal{M}_-)$ and $W^s(\mathcal{M}_+)$ with Σ_+ by $Q(\mathcal{M}_-)$ respectively $Q^{-1}(\mathcal{M}_+)$, see Figure 1. Likewise, we define $Q(\mathcal{M}_+)$ and $Q^{-1}(\mathcal{M}_-)$ in Σ_- . For the moment we focus on the intersections with Σ_+ . The first heteroclinic connections through Σ_+ correspond to zeros of the following time-dependent distance function (here ξ serves as the ‘time’):

$$(2.3) \quad \Delta W_+(\xi, p_0, q_0) = \begin{pmatrix} v_+(\xi) \\ f(p_0)(u_+^3(\xi) - u_+(\xi)) \end{pmatrix} \wedge \begin{pmatrix} \frac{\partial}{\partial \varepsilon}[u_\varepsilon^u(\xi) - u_\varepsilon^s(\xi)]|_{\varepsilon=0} \\ \frac{\partial}{\partial \varepsilon}[v_\varepsilon^u(\xi) - v_\varepsilon^s(\xi)]|_{\varepsilon=0} \end{pmatrix},$$

where the wedge product represents the scalar cross-product in the plane. The solutions $\gamma_\varepsilon^u(\xi) = (u_\varepsilon^u(\xi), v_\varepsilon^u(\xi), p_\varepsilon^u(\xi), q_\varepsilon^u(\xi))$ in $W^u(\mathcal{M}_-)$ and $\gamma_\varepsilon^s(\xi) = (u_\varepsilon^s(\xi), v_\varepsilon^s(\xi), p_\varepsilon^s(\xi), q_\varepsilon^s(\xi))$ in $W^s(\mathcal{M}_+)$ of equations (1.7) are determined by the initial condition $\gamma_\varepsilon^{u,s}(0) = (0, v_\varepsilon^{u,s}, p_0, q_0)$; $\gamma_0(\xi) = (u_+(\xi), v_+(\xi), p_0, q_0)$ is defined as the heteroclinic solution (2.2) to the $\varepsilon = 0$ system. Here $u_+(\xi) = u_+(\xi; p_0)$, $v_+(\xi) = v_+(\xi; p_0)$ and $\gamma_0(0) = (0, \frac{1}{2}\sqrt{2f(p_0)}, p_0, q_0)$. The

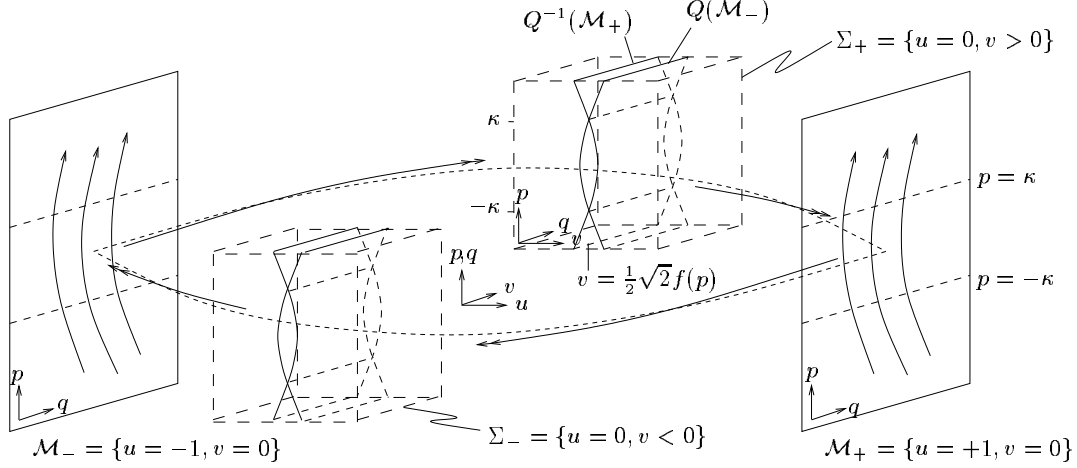


Figure 1: A sketch of the four-dimensional phase space of (1.7) with Melnikov functions $\Delta W_{\pm} = \alpha(p^2 - \kappa^2)$ for constants α and κ . The dashed cycle represents an unperturbed heteroclinic cycle.

$O(\varepsilon)$ splitting distance is given by $\Delta W_+(0, p_0, q_0)$ and depends on the wave speed c ; we therefore denote ΔW_+ by $\Delta W_+(0, p_0, q_0; c)$. The equation (2.3) does not contain any terms from the p_{ξ} , q_{ξ} equations, which illustrates that the splitting distance between the stable and unstable manifolds is only influenced by the fast field. Therefore the perturbations f and g are important here, and k is not.

Similar to the derivation of the adiabatic Melnikov function in systems where a homoclinic manifold is splitted [21], one shows that for the perturbed heteroclinic manifold with $v > 0$ the splitting is given by

$$(2.4) \quad \Delta W_+(0, p_0, q_0; c) = \int_{-\infty}^{\infty} \begin{pmatrix} v_+(\xi) \\ f(p_0)(u_+^3(\xi) - u_+(\xi)) \end{pmatrix} \wedge \begin{pmatrix} 0 \\ m(u_+, v_+, p_0, q_0) \end{pmatrix} d\xi,$$

where

$$(2.5) \quad m(u_+, v_+, p_0, q_0) = -v_+c - g(u_+, v_+, p_0) + \frac{df}{dp}(p_0)(u_+^3 - u_+) \frac{\partial p}{\partial \varepsilon}.$$

Note that the unperturbed heteroclinic solutions depend on p_0 . The function $\frac{\partial p}{\partial \varepsilon}$ satisfies $\frac{\partial p}{\partial \varepsilon}|_{\xi=0} = 0$ and $\frac{d}{d\xi} \left(\frac{\partial p}{\partial \varepsilon} \right) = q_0$, so $\frac{\partial p}{\partial \varepsilon}(\xi) = q_0 \xi$. Clearly only even terms in g contribute to $\Delta W_+(0, p_0, q_0; c)$, since v_+ is even.

In the following a point $x_0 = (0, v_0, p_0, q_0) \in \Sigma_+$ is said to lie *inside* $Q^{-1}(\mathcal{M}_+)$ when its v coordinate satisfies $v_0 < v_1$, where $(0, v_1, p_0, q_0) \in Q^{-1}(\mathcal{M}_+)$ has the same p, q coordinates as x_0 . The point lies *outside* $Q^{-1}(\mathcal{M}_+)$ when $v_0 > v_1$. Similar definitions apply to other manifolds in Σ_{\pm} . Clearly $Q(\mathcal{M}_-)$ lies inside $Q^{-1}(\mathcal{M}_+)$ for (p_0, q_0) with $\Delta W_+(0, p_0, q_0; c) < 0$, and outside $Q^{-1}(\mathcal{M}_+)$ for (p_0, q_0) with $\Delta W_+(0, p_0, q_0; c) > 0$.

Remark 2.1 Similar to the derivation of the function ΔW_+ we can derive a function ΔW_- that measures the splitting distance between $Q(\mathcal{M}_+)$ and $Q^{-1}(\mathcal{M}_-)$ in the hyperplane Σ_- . If the model (1.7) possesses the symmetry $\{u \rightarrow -u, v \rightarrow -v\}$ then $\Delta W_- = \Delta W_+$. Such symmetry is convenient, but not essential for our methods.

Remark 2.2 Although we focus on problems with a Melnikov function having no, one or two zeros, the geometrical techniques we use in section 3 can also be used in systems with Melnikov functions with more than two zeros. This would however involve much more bookkeeping and lead to a more complicated structure.

2.2 The interaction of the slow flow and the fast field

The functions ΔW_- and ΔW_+ give us basic information about the global behaviour in the fast field, and are determined by f and g . The remaining function to address is k , the function that strongly determines the flow on \mathcal{M}_\pm . For $g(\pm 1, 0, p, q) = 0$, this flow is given by

$$\begin{aligned}\dot{p} &= \varepsilon q, \\ \dot{q} &= -\varepsilon k(\pm 1, 0, p, q) - \varepsilon^{1+\nu} c q.\end{aligned}$$

In earlier work, the relative positions of the stable and unstable manifolds and the relative directions of the slow and the fast flows appeared to strongly influence the existence of higher order (n -loop) orbits connecting a slow manifold to itself. We refer to [9, 19] where the relative position of stable and unstable manifolds (‘inner’ and ‘outer’ case) played a rôle, and to [8] and [13] where the relative directions of flows (‘cooperating’ and ‘counteracting’) were important. We first explain the notion of cooperating and counteracting flows in a three-dimensional system and then extend it to the present type of systems.

Consider the system (1.5) with $F_1(0, 0, z; q) = 0$ and, for simplicity, $F_2(0, 0, z; p) > 0$. This system possesses a normally hyperbolic slow manifold $\{x = y = 0\}$ that is for $\varepsilon = 0$ connected to itself by a homoclinic manifold \mathcal{H} filled with families of periodic orbits. Since the perturbed ($\varepsilon > 0$) flow is $O(\varepsilon)$ close to the $\varepsilon = 0$ flow, the flow inside \mathcal{H} is still almost periodic and returns from $\{y = 0, x > 1\}$ to itself.

To define cooperating and counteracting flows we compare the flow on the slow manifold and the averaged flow in the fast field. The flow on the slow manifold is $\dot{z}|_{x=y=0} > 0$. To quantify the contribution of the fast field to the change in z , we define the averaged change in z during one fast excursion from $\{y = 0, x > 1\}$ back to itself as

$$\Delta Z_f = \int_0^{T_\varepsilon} \dot{z} dt = \varepsilon \int_0^{T_\varepsilon} F_2(x_\varepsilon, y_\varepsilon, z_\varepsilon; p) dt,$$

where $(x_\varepsilon(t), y_\varepsilon(t), z_\varepsilon(t))$ is a solution of (1.5) with return time T_ε . Approximating the solution $(x_\varepsilon(t), y_\varepsilon(t), z_\varepsilon(t))$ by an $O(\varepsilon)$ close solution $(x_0(t), y_0(t), z_0)$ of the $\varepsilon = 0$ problem and T_ε by its period T_0 , we obtain

$$(2.6) \quad \Delta Z_f = \varepsilon \int_0^{T_0} F_2(x_0(t), y_0(t), z_0; p) dt + O(\varepsilon^2).$$

Clearly ΔZ_f depends on z_0 . It also depends on the integral $E = \frac{1}{2}y_0^2 - \frac{1}{2}x_0^2 + \frac{1}{3}x_0^3$ of the unperturbed orbit. In the limit $E \uparrow 0$ we approach the unperturbed homoclinic manifold and the integration interval becomes $(-\infty, \infty)$.

We now consider an orbit, parameterized by z_0 , E and p, q , that follows the slow flow on $\{x = y = 0\}$ during a time T_s and makes a loop through the fast field afterwards. During the time T_s z changes with an amount $\Delta Z_s = \int_0^{T_s} \dot{z}|_{x=y=0} dt > 0$. Depending on z_0 , E and p , $\Delta Z_f(z_0, E, p)$ may be positive or negative. In the former case both $\Delta Z_s > 0$ and $\Delta Z_f > 0$, which excludes for instance periodic behaviour. Both fields *cooperate* in this case. In the latter case $\Delta Z_s > 0$ but $\Delta Z_f < 0$, so the slow and fast flows might balance each other and allow for a periodic orbit. Here the flows *counteract*. It has been shown in [8, 13] that this distinction is crucial for the complexity of solutions of (1.5).

We note here, that the expression ΔZ_s is not known in general, since we cannot control the flow near the slow manifold. We however can exploit the fact that orbits exponentially close to a hyperbolic slow manifold follow the flow on this manifold during a time $T_s = O(\frac{1}{\varepsilon})$ before jumping off. This makes $\Delta Z_s(z_0, E, p, q) = O(1)$ for such orbits. The closer an orbit comes to the slow manifold, the longer it follows the flow on it, and thus this $O(1)$ change in z can be arbitrarily large. This is made more explicit in Lemma 2.6.

We now return to system (1.7). The flow on the slow manifolds \mathcal{M}_\pm contributes to the changes in p and q with amounts ΔP_s and ΔQ_s per passage of an orbit through the neighbourhoods of the manifolds. If the ‘time’ spent near the slow manifold is T_s , these expressions are given by

$$\begin{aligned}\Delta P_s|_{\mathcal{M}_\pm} &= \int_0^{T_s} \dot{p}|_{\mathcal{M}_\pm} d\xi = \varepsilon \int_0^{T_s} q(\xi) d\xi, \\ \Delta Q_s|_{\mathcal{M}_\pm} &= \int_0^{T_s} \dot{q}|_{\mathcal{M}_\pm} d\xi = \varepsilon \int_0^{T_s} (-k(\pm 1, 0, p(\xi), q(\xi)) - \varepsilon^\nu c q(\xi)) d\xi.\end{aligned}$$

In these integrals p and q depend on ξ . Note, that ΔP_s is the same on \mathcal{M}_- and \mathcal{M}_+ , and ΔQ_s is independent of \mathcal{M}_\pm if k is symmetric in u . The contributions of the averaged fast flow during one circuit from Σ_+ to Σ_+ through the fast field are $\Delta P_f(p, q, E)$ and $\Delta Q_f(p, q, E)$, with E as defined in (2.1). They can be computed by

$$\begin{aligned}\Delta P_f(p, q, E) &= \int_0^{T_\varepsilon} \dot{p} d\xi = \varepsilon \int_0^{T_\varepsilon} q d\xi, \\ \Delta Q_f(p, q, E) &= \int_0^{T_\varepsilon} \dot{q} d\xi = \varepsilon \int_0^{T_\varepsilon} (-k(u(\xi), v(\xi), p, q) - \varepsilon^\nu c q) d\xi,\end{aligned}$$

where T_ε is the return ‘time’, and p and q serve as parameters. In §2.3 we omit the subscript f and in section 3 we approximate solutions and their return time as in (2.6) to estimate these integrals in some examples. If $\Delta P_f(p, q, E)$ and $\Delta Q_f(p, q, E)$ have the same sign as respectively ΔP_s and ΔQ_s on both \mathcal{M}_- and \mathcal{M}_+ , the flow is always in one well-defined direction with respect to p and q . In this situation we say that the fast and slow flows *cooperate*. Clearly no periodic orbits can exist in this case.

If $\text{sign } \Delta P_f(p, q, E) = -\text{sign } \Delta P_s|_{\mathcal{M}_\pm}$ and $\text{sign } \Delta Q_f(p, q, E) = -\text{sign } \Delta Q_s|_{\mathcal{M}_\pm}$, a balance between both flows, possibly allowing for periodic orbits, can occur. In both the p and the q direction the fast flow is opposite to the flow on both slow manifolds. Therefore this clearly is a *counteracting* situation. We will see that many more homoclinic or heteroclinic orbits than in a cooperating situation can exist here. See also [8] and [13].

It is important to notice that the definition of cooperating and counteracting flows in [8] and [13], which we explained for (1.5), was simple since the system there possessed only one hyperbolic slow manifold and this manifold was one-dimensional. However, here there are two such manifolds \mathcal{M}_\pm , which can either contain identical flows (or at least flows in the same direction), or flows in different directions. In the latter case the fast flow always cooperates with the flow on the one slow manifold when it counteracts to the flow on the other. Depending on the strength of the flows a balance might be possible.

Since \mathcal{M}_\pm are two-dimensional, the slow flow might cooperate with the fast flow in one direction but counteract in the other direction. Of course periodic orbits cannot exist then, but a system with this behaviour can still possess many more homoclinic and heteroclinic orbits than a fully cooperating system. We will illustrate this with examples in sections 3 and 4.

The slow and the fast parts of orbits $\gamma_\pm^u(\xi)$ in $W^u(\mathcal{M}_\pm)$ or $\gamma_\pm^s(\xi)$ in $W^s(\mathcal{M}_\pm)$ are related to each other by the *base-points* of the Fenichel fibers in $W^u(\mathcal{M}_\pm)$ or $W^s(\mathcal{M}_\pm)$ that we will describe here. Consider $\gamma_+^s(\xi) \subset W^s(\mathcal{M}_+)$ with $\gamma_+^s(0) \in Q^{-1}(\mathcal{M}_+) \subset \{u = 0\}$. By geometrical singular perturbation theory [11, 15] there is an orbit $\gamma_{\mathcal{M}_+}^s(\xi; p_0^s, q_0^s) \subset \mathcal{M}_+$ with $\gamma_{\mathcal{M}_+}^s(0; p_0^s, q_0^s) = (p_0^s, q_0^s) \in \mathcal{M}_+$, such that $\|\gamma_+^s(\xi) - \gamma_{\mathcal{M}_+}^s(\xi; p_0^s, q_0^s)\|$ is exponentially small for $\xi > 0$ with $\xi \geq O(\frac{1}{\varepsilon})$. The orbit $\gamma_{\mathcal{M}_+}^s(\xi; p_0^s, q_0^s)$ determines the behaviour of $\gamma_+^s(\xi)$ near \mathcal{M}_+ . The points $(p_0^s, q_0^s) \in \mathcal{M}_\pm$ and $(p_0^u, q_0^u) \in \mathcal{M}_\pm$ (which are defined analogously) are the so-called base-points, where the orbits in $W^s(\mathcal{M}_\pm)$ and $W^u(\mathcal{M}_\pm)$ respectively ‘touch down’ on \mathcal{M}_\pm and ‘take off’ from \mathcal{M}_\pm (see also [10, 7]). The orbits in $W^s(\mathcal{M}_\pm)$ and $W^u(\mathcal{M}_\pm)$ can be parameterized by their base-points.

Whenever an orbit $\gamma(\xi)$ temporarily ‘touches down’ on \mathcal{M}_\pm to follow the slow flow during a certain time $T_s = O(\frac{1}{\varepsilon})$ as above and ‘takes off’ again after this time, the behaviour of this orbit near \mathcal{M}_\pm is determined by one particular orbit $\gamma_{\mathcal{M}_\pm}$ too. This orbit contains both a touch down point and a take off point for $\gamma(\xi)$. The position of the base-points can be computed explicitly; see [10, 7].

2.3 Basic tools to further describe the structure of the phase space

In the present subsection we introduce some basic tools that will be applied in the rest of the paper. These tools will be used to construct further heteroclinic or homoclinic orbits with more than one jumps through the fast field. These orbits will be referred to as higher order connections.

Since the unperturbed flow contains families of periodic orbits inside $\mathcal{H}_+ \cup \mathcal{H}_-$, a Poincaré return map for the part of the perturbed flow inside an $O(\varepsilon)$ neighbourhood of $\mathcal{H}_+ \cup \mathcal{H}_-$ can be defined, as we in essence already sketched in §2.2. The planes Σ_\pm are both candidates for the Poincaré cross section to the flow.

We concentrate on Σ_+ and define the Poincaré return map $\mathcal{P}_+ : \Sigma_+ \rightarrow \Sigma_+$ as

$$(2.7) \quad \mathcal{P}_+(E, p, q) = (E + \Delta E(E, p, q), p + \Delta P(E, p, q), q + \Delta Q(E, p, q)).$$

Note that points on Σ_+ are defined by their coordinates (E, p, q) , where E , p and q are the integrals of (1.7). Since the map is only defined in an $O(\varepsilon)$ neighbourhood of the region inside $\mathcal{H}_+ \cup \mathcal{H}_-$, E must satisfy $E \in (0, \frac{1}{4}f(p) + O(\varepsilon))$. The difference ΔP is a combination

of the contributions ΔP_f and ΔP_s . The same applies to ΔQ . Repeated applications of \mathcal{P}_+ , \mathcal{P}_+^{-1} to $Q(\mathcal{M}_-)$ and $Q^{-1}(\mathcal{M}_+)$ will yield further intersections of $W^u(\mathcal{M}_-)$ and $W^s(\mathcal{M}_+)$ with Σ_+ , and give information about the structure of $W^u(\mathcal{M}_-)$ and $W^s(\mathcal{M}_+)$ and about possible intersections $W^u(\mathcal{M}_-) \cap W^s(\mathcal{M}_+)$. We define and use the map $\mathcal{P}_- : \Sigma_- \rightarrow \Sigma_-$ in the same way.

These Poincaré maps will only be useful to construct orbits that take off from \mathcal{M}_- , pass Σ_+ , make several circuits through the fast field back to Σ_+ , and finally touch down on \mathcal{M}_+ (or take off from \mathcal{M}_+ and touch down on \mathcal{M}_-). To investigate homoclinic orbits, that take off from and touch down on one and the same slow manifold, we also need to map from Σ_+ to Σ_- or vice versa. Therefore we introduce the ‘half’ Poincaré maps $Q_+ : \Sigma_+ \rightarrow \Sigma_-$ and $Q_- : \Sigma_- \rightarrow \Sigma_+$ such that $Q_- \circ Q_+ = \mathcal{P}_+$ and $Q_+ \circ Q_- = \mathcal{P}_-$. We also define for $n > 1$:

$$\begin{aligned} Q^{2n+1}(\mathcal{M}_-) &\equiv (Q_- \circ Q_+)^n \circ Q(\mathcal{M}_-) \subset \Sigma_+, \\ Q^{2n}(\mathcal{M}_-) &\equiv Q_+ \circ (Q_- \circ Q_+)^{n-1} \circ Q(\mathcal{M}_-) \subset \Sigma_-, \\ Q^{-2n-1}(\mathcal{M}_+) &\equiv (Q_+^{-1} \circ Q_-^{-1})^n \circ Q^{-1}(\mathcal{M}_+) \subset \Sigma_+, \\ Q^{-2n}(\mathcal{M}_+) &\equiv Q_-^{-1} \circ (Q_+^{-1} \circ Q_-^{-1})^{n-1} \circ Q^{-1}(\mathcal{M}_+) \subset \Sigma_-. \end{aligned}$$

$Q^m(\mathcal{M}_+)$ and $Q^{-m}(\mathcal{M}_-)$ are defined similarly.

The following lemmas and corollary describe how \mathcal{P}_+ acts on points at a distance d , $d = O(\varepsilon)$, from $Q^{-1}(\mathcal{M}_+)$, and how \mathcal{P}_+^{-1} acts on points at a distance d from $Q(\mathcal{M}_-)$. They will be used to describe $W^{u,s}(\mathcal{M}_\pm)$ globally by further intersections with Σ_+ .

Lemma 2.3 is a general lemma, from which we derive Corollary 2.4. We refer to [11, 15, 8] for proofs. It describes orbits that start at Σ_+ , pass through a neighbourhood of \mathcal{M}_+ and finally arrive at Σ_- .

Lemma 2.3 *Consider a system*

$$\begin{aligned} \dot{u} &= f_0(u, v, w) + \varepsilon f_1(u, v, w), \\ (2.8) \quad \dot{v} &= g_0(u, v, w) + \varepsilon g_1(u, v, w), \\ \dot{w} &= \varepsilon h_1(u, v, w), \end{aligned}$$

where $\dot{} = \frac{d}{dt}$, the variables u and v are scalars and w is allowed to be a vector quantity. Assume that the $\varepsilon = 0$ system possesses a compact, normally hyperbolic, invariant slow manifold Γ_0 with stable and unstable manifolds $W^s(\Gamma_0)$ and $W^u(\Gamma_0)$. Define local manifolds $W_{\text{loc}}^s(\Gamma_0) = W^s(\Gamma_0) \cap \mathcal{B}$ and $W_{\text{loc}}^u(\Gamma_0) = W^u(\Gamma_0) \cap \mathcal{B}$ where \mathcal{B} is a compact neighbourhood of Γ_0 . Put $0 \leq \varepsilon \ll 1$.

Then there is a normally hyperbolic slow manifold Γ_ε with local stable and unstable manifolds $W_{\text{loc}}^s(\Gamma_\varepsilon)$ and $W_{\text{loc}}^u(\Gamma_\varepsilon)$ $O(\varepsilon)$ close to the local stable and unstable manifolds of Γ_0 . Moreover, if $d(q_0, W_{\text{loc}}^s(\Gamma_\varepsilon)) = d = O(\varepsilon)$ for a point $q_0 = (u(0), v(0), w(0))$ in \mathcal{B} then the orbit $\gamma_\varepsilon(t)$ with $\gamma_\varepsilon(0) = q_0$ passes Γ_ε and leaves \mathcal{B} at some $t = T$ such that the estimate $d(\gamma_\varepsilon(T), W_{\text{loc}}^u(\Gamma_\varepsilon)) = O(d)$ holds. Similarly, for the reversed flow, if $d(q_0, W_{\text{loc}}^u(\Gamma_\varepsilon)) = d$ then the orbit $\gamma_\varepsilon(t)$ with $\gamma_\varepsilon(0) = q_0$ passes Γ_ε and leaves \mathcal{B} at time $t = -T$ with $d(\gamma_\varepsilon(-T), W_{\text{loc}}^s(\Gamma_\varepsilon)) = O(d)$.

Here $d(\cdot, \cdot)$ is the standard distance function. For solutions with $E < \frac{1}{4}f(p) + O(\varepsilon)$ spend only $O(1)$ time outside the neighbourhoods of \mathcal{M}_\pm , this lemma immediately implies for system (1.7):

Corollary 2.4 *Assume $d = O(\varepsilon)$. If $d(x_0, Q^{-1}(\mathcal{M}_+)) = d$ for a point $x_0 = (u, v, p, q)$ with $E(x_0) < \frac{1}{4} + O(\varepsilon)$, then $d(Q_+(x_0), Q(\mathcal{M}_+)) = O(d)$. Similarly, if $d(x_0, Q(\mathcal{M}_+)) = d$ for a point $x_0 = (u, v, p, q)$ with $E(x_0) < \frac{1}{4} + O(\varepsilon)$, then $d(Q_+^{-1}(x_0), Q^{-1}(\mathcal{M}_+)) = O(d)$.*

Of course, Q_- acts analogously.

The neighbourhood \mathcal{B} is determined by the Fenichel normal form for the system and can be chosen to be a box in the fast Fenichel coordinates (a and b , see (2.9)), say $\mathcal{B} = \{(a, b, w) | 0 \leq a \leq \Delta, 0 \leq b \leq \Delta\}$ where $1 \gg \Delta \gg \varepsilon > 0$ is a constant independent of ε , chosen such that the fast flow in (2.8) is $O(1)$ with respect to Δ . This normal form is used to study the behaviour inside \mathcal{B} (see for instance [15]). We here derive the Fenichel normal form for equation (2.8). The eigenvalues in the fast directions (so $O(1)$ with respect to ε) for the linearization about a point $(u, v, w) \in \Gamma_\varepsilon$ are λ_\pm with $\lambda_+ > 0$ and $\lambda_- < 0$ since Γ_ε is normally hyperbolic. According to Fenichel [11] C^r coordinate transformations exist, such that locally (within \mathcal{B}) the stable and unstable manifolds correspond to the coordinate axes in the stable and unstable directions and (2.8) can be rewritten as

$$(2.9) \quad \begin{aligned} \dot{a} &= \lambda_+ a + F(a, b, w, \varepsilon)a, \\ \dot{b} &= \lambda_- b + G(a, b, w, \varepsilon)b, \\ \dot{w} &= \varepsilon H(a, b, w, \varepsilon). \end{aligned}$$

within \mathcal{B} . Clearly $\{a = 0\}$ and $\{b = 0\}$ are the local invariant manifolds. The functions F and G contain linear and higher order terms in a and b , as well as $O(\varepsilon)$ terms. H is an equivalent of h_1 .

Lemma 2.3 immediately yields estimates on the time of flight and the change in w within the box \mathcal{B} . They are given in the next lemma (see also [8]).

Lemma 2.5 *For a solution entering \mathcal{B} at $t = t_{\text{in}}$ with $b_{\text{in}} = \Delta$, $a_{\text{in}} = d$ with $|\log d| \ll \frac{1}{\varepsilon}$ the time of flight T between entrance in and exit at $t = t_{\text{out}}$ from \mathcal{B} is*

$$T = O(|\log d|);$$

during this time T the w coordinate of the solution changes with an amount

$$\Delta w = O(\varepsilon |\log d|).$$

Corollary 2.4 does not suffice to describe an orbit that enters a neighbourhood of one of the manifolds \mathcal{M}_\pm exponentially close to a stable manifold $W^s(\mathcal{M}_\pm)$. In the neighbourhood of a given trajectory in \mathcal{M}_\pm (that is not a fixed point or an entire periodic orbit) the slow flow on \mathcal{M}_\pm can be rectified by coordinate changes $(p, q) \rightarrow (r, s)$ such that orbits on \mathcal{M}_\pm are (locally) determined by $\dot{r} = \varepsilon R$ and $\dot{s} = 0$. If moreover the foliations of the stable and unstable manifolds, parameterized by points on the slow manifolds, are straightened, the equations on the stable and unstable manifolds are determined by those on the slow manifold. In other words, the flow on $W^{u,s}(\mathcal{M}_\pm)$ then also satisfies $\dot{r} = \varepsilon R$ and $\dot{s} = 0$. See for instance [17, 16]. For system (1.7) this locally transforms the normal form (2.9) in the neighbourhoods \mathcal{B}_\pm of \mathcal{M}_\pm to

$$\begin{aligned} \dot{a} &= \lambda_+ a + \tilde{F}(a, b, r, s, \varepsilon)a, \\ \dot{b} &= \lambda_- b + \tilde{G}(a, b, r, s, \varepsilon)b, \\ \dot{r} &= \varepsilon(R + H_1(a, b, r, s, \varepsilon)ab), \\ \dot{s} &= \varepsilon H_2(a, b, r, s, \varepsilon)ab. \end{aligned}$$

By [16] orbits that enter \mathcal{B}_\pm at $s = s_0, r = r_0$ $O(e^{-\frac{\kappa}{\varepsilon}})$ C^1 -close to $W^s(\mathcal{M}_\pm)$ for some constant κ , leave \mathcal{B}_\pm after $O(\frac{1}{\varepsilon})$ time $O(e^{-\frac{\kappa}{\varepsilon}})$ C^1 -close to $W^u(\mathcal{M}_\pm)$ and to $\{s = s_0\}$. The r coordinate may change with an $O(1)$ amount. We formulate this as

Lemma 2.6 *Solutions to (1.7) that enter \mathcal{B}_\pm $O(e^{-\frac{\kappa}{\varepsilon}})$ C^1 -close to $W^s(\mathcal{M}_\pm)$ with $(p, q) = (p_0, q_0)$ stay $O(e^{-\frac{\kappa}{\varepsilon}})$ close to the orbit through $(\pm 1, 0, p_0, q_0)$ in \mathcal{M}_\pm for an $O(1)$ distance, and leave \mathcal{B}_\pm $O(e^{-\frac{\kappa}{\varepsilon}})$ C^1 -close to $W^u(\mathcal{M}_\pm)$.*

3 Global geometry, a ‘trivial’ example

In this section we analyse one of the simplest models of the form (1.1) with F as in (1.4) to illustrate our theory. It has a perturbation G that is quadratic in P and is reminiscent of the perturbation in the \dot{y} -equation of the systems studied in [8, 13]. The reaction term K in the equation for P is constant. We will conclude that the simplest choice $K = 1$ already leads to very complicated behaviour. The system of our concern is

$$(3.1) \quad \begin{aligned} U_t &= U_{xx} - U^3 + U - \varepsilon U_x(P^2 + a), \\ P_t &= P_{xx} - \varepsilon^2, \end{aligned}$$

leading to the ODE

$$(3.2) \quad \begin{aligned} u_\xi &= v, \\ v_\xi &= u^3 - u + \varepsilon v(p^2 + a - c), \\ p_\xi &= \varepsilon q, \\ q_\xi &= \varepsilon(1 - cq). \end{aligned}$$

Note, that we chose $\nu = 0$ in (1.1) and that a choice $\nu > 0$ would have lead to a higher order term in the q_ξ equation. The slow flow in this system is completely decoupled and is always given by

$$(3.3) \quad \begin{aligned} p_\xi &= \varepsilon q, \\ q_\xi &= \varepsilon(1 - cq). \end{aligned}$$

This means in particular, that the flows on the manifolds \mathcal{M}_\pm are identical, and that the orbits in \mathcal{M}_\pm are determined by $\frac{dp}{dq} = \frac{q}{1-cq}$. Another consequence is, that for $c \neq 0$ the hyperplane $\{q = \frac{1}{c}\}$ is invariant under the flow.

Filling in the choices for f , g and k in (2.4) and straightforward integration give the Melnikov functions

$$\Delta W_\pm(0, p_0, q_0; c) = \frac{2}{3}\sqrt{2}(p_0^2 + a - c).$$

The system (3.2) possesses the symmetry

$$(3.4) \quad \{u \rightarrow -u, v \rightarrow -v\}$$

as discussed in Remark 2.1, so $\Delta W_+ = \Delta W_-$, and thus \mathcal{Q}_+ and \mathcal{Q}_- are similar. More precisely,

$$(3.5) \quad \mathcal{Q}_- = I_+^{-1} \circ \mathcal{Q}_+ \circ I_-,$$

where I_{\pm} are ‘identity’ maps

$$(3.6) \quad I_- : \Sigma_- \rightarrow \Sigma_+, \quad I_+ : \Sigma_+ \rightarrow \Sigma_-, \quad I_{\pm}(0, v, p, q) = (0, -v, p, q).$$

To find a complete global structure we need to apply both Q_+ and Q_- since multi-jump orbits cross both Σ_+ and Σ_- and make full circuits through the fast field. The above identity however enables us to restrict our investigations to one of them.

$\Delta W_{\pm}(0, p_0, q_0; c) = 0$ for $p_0 = \pm\sqrt{c-a}$ ($c-a \geq 0$), which implies that for $\varepsilon > 0$, small enough, and $c-a > 0$ the manifolds $W^u(\mathcal{M}_-)$ and $W^s(\mathcal{M}_+)$, respectively $W^u(\mathcal{M}_+)$ and $W^s(\mathcal{M}_-)$, intersect in a 2-dimensional, transverse way, $O(\varepsilon)$ close to the hyperplanes $\{p_0 = \pm\sqrt{c-a}\}$. These intersections correspond to families of heteroclinic orbits $\gamma_h^{\pm}(\xi; q)$ and $\tilde{\gamma}_h^{\pm}(\xi; q)$ that make a jump through the fast field near one of the intersection planes. These families are parameterized by q . See Figure 1. In the original PDE context each heteroclinic orbit corresponds to a front that connects $U = -1$ with $U = +1$ and travels with a speed c ; see Figure 7 in section 5. We define orbits $\gamma_h^{\pm}(\xi; q)$ and $\tilde{\gamma}_h^{\pm}(\xi; q)$ where $\gamma_h^{\pm}(0; q) \in \Sigma_+$, $\tilde{\gamma}_h^{\pm}(0; q) \in \Sigma_-$. The former orbits satisfy $\lim_{\xi \rightarrow \infty} d(\gamma_h^{\pm}(\xi; q), \mathcal{M}_+) = 0$, $\lim_{\xi \rightarrow -\infty} d(\gamma_h^{\pm}(\xi; q), \mathcal{M}_-) = 0$, the latter satisfy $\lim_{\xi \rightarrow \infty} d(\tilde{\gamma}_h^{\pm}(\xi; q), \mathcal{M}_-) = 0$, $\lim_{\xi \rightarrow -\infty} d(\tilde{\gamma}_h^{\pm}(\xi; q), \mathcal{M}_+) = 0$. The indices \pm in the notation denote whether an orbit jumps with positive or negative v , the parameter q relates an orbit to the q -coordinate of its take off base-point in \mathcal{M}_{\pm} , as described in §2.2. The base points can be parameterized by only their q -coordinates since they correspond to Fenichel fibers in $W^u(\mathcal{M}_{\pm})$ that lie in the transverse intersection of $W^u(\mathcal{M}_{\pm})$ and $W^s(\mathcal{M}_{\pm})$.

Remark 3.1 Since \mathcal{M}_{\pm} are not compact, one has to be careful with these limits. The perturbations in (3.2) are quadratic in p and linear q , so they are no longer singular perturbations for p or q large ($O(\frac{1}{\sqrt{\varepsilon}})$ or $O(\frac{1}{\varepsilon})$ respectively), and \mathcal{M}_{\pm} thus cannot be interpreted as a slow manifold for large p, q . Also, Fenichel theory can only be applied for compact manifolds. However, compact submanifolds of \mathcal{M}_{\pm} may be considered instead. See the discussion in section 6.

Let $p^{\pm}(q) = \pm\sqrt{c-a} + O(\varepsilon)$ denote the exact p values for which $Q(\mathcal{M}_{\pm})$ and $Q^{-1}(\mathcal{M}_{\pm})$ intersect, parameterized by q . For general G in (1.6) that depends on both P and P_x , or for $f(P) \neq \text{const.}$ the parameterization by q would have a leading order effect, but here it only appears in the $O(\varepsilon)$ terms. For $c-a=0$ and arbitrary q , ΔW_{\pm} have a double zero $p=0$, which implies by $\Delta W_{\pm}(0, 0, q; c) = \frac{\partial}{\partial p} \Delta W_{\pm}(0, 0, q; c) = 0$, $\frac{\partial^2}{\partial p^2} \Delta W_{\pm}(0, 0, q; c) \neq 0$, $\frac{\partial}{\partial c} \Delta W_{\pm}(0, 0, q; c) \neq 0$, that for each a, q fixed a unique value $c = c^*(a, q) = a + \tilde{c}(q)$ with $\tilde{c}(q) = O(\varepsilon)$ exists for which the restricted manifolds $W^u(\mathcal{M}_-)|_q$ and $W^s(\mathcal{M}_+)|_q$, resp. $W^u(\mathcal{M}_+)|_q$ and $W^s(\mathcal{M}_-)|_q$, have quadratic contact in a hyperplane with constant q . When $c < c^*(a, q)$ for all q , the stable and unstable manifolds do not intersect; when $c > c^*(a, q)$ for all q , both $Q(\mathcal{M}_-)$ and $Q^{-1}(\mathcal{M}_+)$, and $Q(\mathcal{M}_+)$ and $Q^{-1}(\mathcal{M}_-)$, intersect each other in two curves. In other words, for a fixed $c^*(a, q)$ is the speed for which a heteroclinic bifurcation takes place in a fixed hyperplane with constant q .

By construction, $|v_{\varepsilon}^u| < |v_{\varepsilon}^s|$ in Σ_{\pm} when $\Delta W_{\pm}(0, p, q; c) < 0$, respectively $|v_{\varepsilon}^u| > |v_{\varepsilon}^s|$ when $\Delta W_{\pm}(0, p, q; c) > 0$. Thus the structure of $Q(\mathcal{M}_-)$ and $Q^{-1}(\mathcal{M}_+)$ in Σ_+ is as in Figure 1 with $\kappa^2 = c-a = O(1) > 0$ and $\alpha = \frac{2}{3}\sqrt{2}$.

3.1 The Poincaré maps

We approximate the Poincaré map \mathcal{P}_+ to investigate the flow inside the parts of $W^{u,s}(\mathcal{M}_\pm)$ that are $O(\varepsilon)$ close to $\mathcal{H}_+ \cup \mathcal{H}_-$. A solution with initial data (E_0, p_0, q_0) on Σ_+ returns to Σ_+ after a ‘time’ $T_\varepsilon(E_0, p_0, q_0)$. The quantities $\Delta E(E_0, p_0, q_0)$, $\Delta P(E_0, p_0, q_0)$ and $\Delta Q(E_0, p_0, q_0)$ measure the accumulated change in the variables E , p and q within this time interval. Thus,

$$\begin{aligned}\Delta E(E_0, p_0, q_0) &= \int_0^{T_\varepsilon} \dot{E}(u_\varepsilon, v_\varepsilon, p_\varepsilon, q_\varepsilon) d\xi = \varepsilon \int_0^{T_\varepsilon} v_\varepsilon^2 (p_\varepsilon^2 + a - c) d\xi, \\ \Delta P(E_0, p_0, q_0) &= \int_0^{T_\varepsilon} \dot{p}(u_\varepsilon, v_\varepsilon, p_\varepsilon, q_\varepsilon) d\xi = \varepsilon \int_0^{T_\varepsilon} q_\varepsilon d\xi, \\ \Delta Q(E_0, p_0, q_0) &= \int_0^{T_\varepsilon} \dot{q}(u_\varepsilon, v_\varepsilon, p_\varepsilon, q_\varepsilon) d\xi = \varepsilon \int_0^{T_\varepsilon} v_\varepsilon^2 (1 - cq_\varepsilon) d\xi,\end{aligned}$$

where $(u_\varepsilon, v_\varepsilon, p_\varepsilon, q_\varepsilon)$ is the solution of (3.2) with the above initial data. We derive an expression for ΔE approximating $(u_\varepsilon(\xi), v_\varepsilon(\xi), p_\varepsilon(\xi), q_\varepsilon(\xi))$ by $(u_0(\xi), v_0(\xi), p_0, q_0)$, the solution of the fast reduced limit problem (i.e. $\varepsilon = 0$ in (3.2)) with the same initial data. This yields

$$\Delta E(E_0, p_0, q_0) = \varepsilon \int_0^{T_0(E_0)} v_0^2 (p_0^2 + a - c) d\xi + O(\varepsilon^2),$$

where $T_0(E_0)$ is the period of the unperturbed periodic solution with $E = E_0$. Unlike the general case, E does not depend on p_0 in system (3.2).

A change of variables, using (2.1), gives

$$\Delta E(E_0, p_0, q_0) = 2\varepsilon \int_{u_m}^{u_p} (p_0^2 + a - c) \sqrt{\frac{1}{2}u^4 - u^2 + 2E_0} du + O(\varepsilon^2),$$

where u_m and u_p are the intersection points of the orbit corresponding to E_0 with $\{v = 0, u < 0\}$ and $\{v = 0, u > 0\}$ respectively. Analogously, one derives

$$\begin{aligned}\Delta P(E_0, p_0, q_0) &= 2\varepsilon \int_{u_m}^{u_p} \frac{q_0}{\sqrt{\frac{1}{2}u^4 - u^2 + 2E_0}} du + O(\varepsilon^2), \\ \Delta Q(E_0, p_0, q_0) &= 2\varepsilon \int_{u_m}^{u_p} \frac{1 - cq_0}{\sqrt{\frac{1}{2}u^4 - u^2 + 2E_0}} du + O(\varepsilon^2).\end{aligned}$$

To obtain more convenient expressions for these integrals we define

$$(3.7) \quad T_i(E) = \oint \frac{u^i}{\sqrt{\frac{1}{2}u^4 - u^2 + 2E}} du,$$

$$(3.8) \quad S_i(E) = \oint u^i \sqrt{\frac{1}{2}u^4 - u^2 + 2E} du,$$

where the integration is over a contour in the complex plane \mathbf{C} that contains the interval $[u_m, u_p]$. In general these expressions depend on $f(p)$ as in the Appendix, but here $f(p) \equiv 1$. We also introduce

$$\tilde{T}_2(E) = T_0(E) - T_2(E) = \oint \frac{1 - u^2}{\sqrt{\frac{1}{2}u^4 - u^2 + 2E}} du.$$

The integrand of this expression becomes zero when $u \rightarrow \pm\infty$, so the limit $\lim_{E \uparrow \frac{1}{4}} \tilde{T}_2(E)$ near the saddles in the $\varepsilon = 0$ system is bounded, while $\lim_{E \uparrow \frac{1}{4}} T_2(E)$ diverges. This bounded expression enables us to find an asymptotic formula for $T_0(E)$ in the neighbourhood of $E = \frac{1}{4}$, which corresponds to the neighbourhood of the unperturbed heteroclinic manifolds \mathcal{H}_\pm and the slow manifolds \mathcal{M}_\pm (see the Appendix). With these notations we end up with

$$(3.9) \quad \Delta E(E, p, q) = \varepsilon(p^2 + a - c)S_0(E) + O(\varepsilon^2),$$

$$(3.10) \quad \Delta P(E, p, q) = \varepsilon q T_0(E) + O(\varepsilon^2),$$

$$(3.11) \quad \Delta Q(E, p, q) = \varepsilon(1 - cq)T_0(E) + O(\varepsilon^2).$$

These expressions provide us with approximations for the Poincaré maps \mathcal{P}_+ (2.7) and \mathcal{P}_- near \mathcal{H}_+ and \mathcal{H}_- .

From these approximations it is immediately clear that periodic orbits do not exist in (3.2), since $T_0(E) \neq 0$ and hence $\Delta P = \Delta Q = 0$ is not possible.

3.2 Existence of n -jump homoclinic or heteroclinic orbits

We investigate the global geometry of the manifolds $W^{u,s}(\mathcal{M}_\pm)$ in (3.2). The geometry in the invariant hyperplane $\{p = \frac{1}{c}\}$ ($c \neq 0$) will be useful to illustrate the geometry of the full system.

It is immediately clear that $\Delta P > 0$ for $q > 0$, and $\Delta P < 0$ for $q < 0$. If $c = 0$, then $\Delta Q > 0$ always; if $c > 0$, then $\Delta Q < 0$ for $q > \frac{1}{c}$ and $\Delta Q > 0$ for $q < \frac{1}{c}$; if $c < 0$, then $\Delta Q < 0$ for $q < \frac{1}{c}$ and $\Delta Q > 0$ for $q > \frac{1}{c}$.

Throughout the remainder of this section we assume $c > 0$ without any restriction. The properties we prove have straightforward analogues for $c < 0$. The map \mathcal{Q}_+ is only well defined for points on $Q(\mathcal{M}_-)$ on orbits that will reach Σ_- in forward ‘time’ ξ . These are exactly the points that lie inside $Q^{-1}(\mathcal{M}_+)$. If $c \leq a$ there is no part of $Q(\mathcal{M}_-)$ inside $Q^{-1}(\mathcal{M}_+)$ and no higher order intersections can exist. Therefore we choose $c > a$ and $c - a = O(1)$. We are interested in the flow in the neighbourhood of the region $\{p^2 \leq c - a\}$, and consider only $p, q = O(1)$ with respect to ε .

The orbits in $\{q = \frac{1}{c}\}$ form a three-dimensional sub-system by the invariance of that hyperplane. To study this sub-system we consider a fixed speed $c > 0$ and vary a . We define

$$\Gamma_\pm \stackrel{\text{def}}{=} \{q = \frac{1}{c}, u = \pm 1, v = 0\} \subset \mathcal{M}_\pm$$

and call their stable and unstable manifolds $W^s(\Gamma_\pm)$ and $W^u(\Gamma_\pm)$ respectively, to obtain a system similar to the one studied in [8, 13]. Instead of one, as in [8, 13], there are two slow manifolds here, but both contain an upward flow ($\dot{p} > 0$) which makes them similar to the slow manifold in [8, 13]. We define restricted Poincaré sections $\sigma_\pm = \Sigma_\pm \cap \{q = \frac{1}{c}\}$ and restrict the maps \mathcal{Q}_+ and \mathcal{Q}_- to these planes. Moreover we define the intersection $W^u(\Gamma_-) \cap \sigma^+$ by $Q(\Gamma_-)$, etc. Note that the Melnikov function gives intersection *points* $W^u(\Gamma_-) \cap W^s(\Gamma_+)$ in σ^+ and $W^u(\Gamma_+) \cap W^s(\Gamma_-)$ in σ^- , $O(\varepsilon)$ close to $\sigma^\pm \cap \{p = \pm\sqrt{c - a}\}$

if $c - a > 0$. Recall that $p^\pm(\frac{1}{c}) = \pm\sqrt{c-a} + O(\varepsilon)$ are defined as the exact p -coordinates of the intersections in $\{q = \frac{1}{c}\}$.

Theorem 3.2 *Consider (3.2). For $c > 0$, $c - a = O(1) > 0$, and all $n = O(|\log \varepsilon|)$ four n -jump homoclinic or heteroclinic solutions of the following type exist in $\{q = \frac{1}{c}\}$:*

two solutions $\gamma_h^i(\xi; \frac{1}{c}, n)$, $i = 1, 2$, with $\lim_{\xi \rightarrow -\infty} d(\gamma_h^i(\xi), \mathcal{M}_-) = 0$,

two solutions $\tilde{\gamma}_h^i(\xi; \frac{1}{c}, n)$, $i = 1, 2$, with $\lim_{\xi \rightarrow -\infty} d(\tilde{\gamma}_h^i(\xi), \mathcal{M}_+) = 0$.

For n odd, the solutions are heteroclinic orbits between \mathcal{M}_+ and \mathcal{M}_- or vice versa, for n even they are homoclinic to \mathcal{M}_+ or \mathcal{M}_- . One of each pair $\gamma_h^i(\xi; \frac{1}{c}, n)$ or $\tilde{\gamma}_h^i(\xi; \frac{1}{c}, n)$ makes all its jumps near $p = +\sqrt{c-a}$, the other makes one jump near $p = -\sqrt{c-a}$ and the next $n-1$ jumps near $p = +\sqrt{c-a}$.

Remark 3.3 Without proof we state that Theorem 3.2 is also valid for $c < 0$, with the remark that the n and $n-1$ jumps take place near $p = -\sqrt{c-a}$ now, while the first jump of the second orbit is near $p = +\sqrt{c-a}$.

Remark 3.4 The symmetry (3.4) allows us to construct from each orbit γ_h its symmetrical counterpart $\tilde{\gamma}_h$, so an existence proof for only the solutions γ_h suffices.

We first analyse the structures of $W^{u,s}(\Gamma_\pm)$ and then use the obtained information to prove Theorem 3.2. Throughout we use the notation $p^\pm = p^\pm(\frac{1}{c})$.

Applying \mathcal{Q}_+ to points on $Q(\Gamma_-)$ in its domain, and using Corollary 2.4 and Lemma 2.6, one finds a curve $\mathcal{Q}_+(Q(\Gamma_-)) = Q^2(\Gamma_-)$ as follows. The largest part of $Q(\Gamma_-)$ inside $Q^{-1}(\Gamma_+)$ lies $O(\varepsilon)$ away from $Q^{-1}(\Gamma_+)$, i.e. $d(x_0, Q^{-1}(\mathcal{M}_+)) = O(\varepsilon)$ where $d(\cdot, \cdot)$ is the standard Euclidean distance. Points x_0 here are mapped inside and $O(\varepsilon)$ away from $Q(\Gamma_+)$ by Corollary 2.4. This corresponds to an $O(\varepsilon)$ change in E . The change in p induced by this mapping can be deduced from (3.10), (A.16) in the Appendix and Lemma 2.5: it is $O(\varepsilon|\log \varepsilon|)$ as long as $q = \frac{1}{c} = O(1)$ and $E - \frac{1}{4}f(p) = E - \frac{1}{4} = O(\varepsilon)$ but not exponentially small. In other words, as long as $d(x_0, Q^{-1}(\mathcal{M}_+)) = O(\varepsilon)$ for $x_0 = (0, v_0, p_0, \frac{1}{c}) \in Q(\Gamma_-)$ inside $Q^{-1}(\Gamma_+)$, its image $\mathcal{Q}_+(x_0) \in \sigma_-$ has coordinates $(0, -v_0, p_0 + O(|\varepsilon \log \varepsilon|), \frac{1}{c})$. However, Lemma 2.6 implies that points on $Q(\Gamma_-)$, inside $Q^{-1}(\Gamma_+)$ but exponentially close to one of the intersection points at $p = p^\pm$, are carried along Γ_+ for $O(\frac{1}{\varepsilon})$ time and $O(1)$ distance. Hence their orbits are stretched upwards along Γ_+ and their images under \mathcal{Q}_+ lie $O(1)$ higher with respect to p ($\dot{p}|_{q=1/c} = \frac{\varepsilon}{c} > 0$) and exponentially close to $Q(\Gamma_+)$. Combining the conclusions for these different sets of points on $Q(\Gamma_-)$ and appealing to continuity, we find that $Q^2(\Gamma_-)$ is a tongue in σ_- as in Figure 2(a).

Applying \mathcal{Q}_-^{-1} to points on $Q^{-1}(\Gamma_+)$ yields two distinct curves $\mathcal{Q}_-^{-1}(Q^{-1}(\Gamma_+)) = Q^{-2}(\Gamma_+)$ by the following arguments. To find the structure of $Q^{-2}(\Gamma_+)$, we first divide $Q^{-1}(\Gamma_+)$ into three parts: the part with $p > p^+$, which lies inside $Q(\Gamma_-)$, the part with $p < p^-$ (inside $Q(\Gamma_-)$ as well), and the part with $p^- < p < p^+$, which has no preimage under \mathcal{M}_+ . When applying \mathcal{Q}_- on the former two parts, we need to consider the backward time direction. Since $\dot{p} = \frac{\varepsilon}{c} > 0$, the p -coordinate will always decrease now. Points with $p > p^+$, or $p < p^-$, inside and $O(\varepsilon)$ close to $Q(\Gamma_-)$ have preimages with about the same (up to $O(|\varepsilon \log \varepsilon|)$) p -coordinate, $O(\varepsilon)$ close to $Q^{-1}(\Gamma_-)$, by Corollary 2.4. Again orbits through points exponentially close to the intersection points $W^u(\Gamma_-) \cap W^s(\Gamma_+)$ are stretched (downwards this time) along Γ_- , and preimages of these points lie exponentially

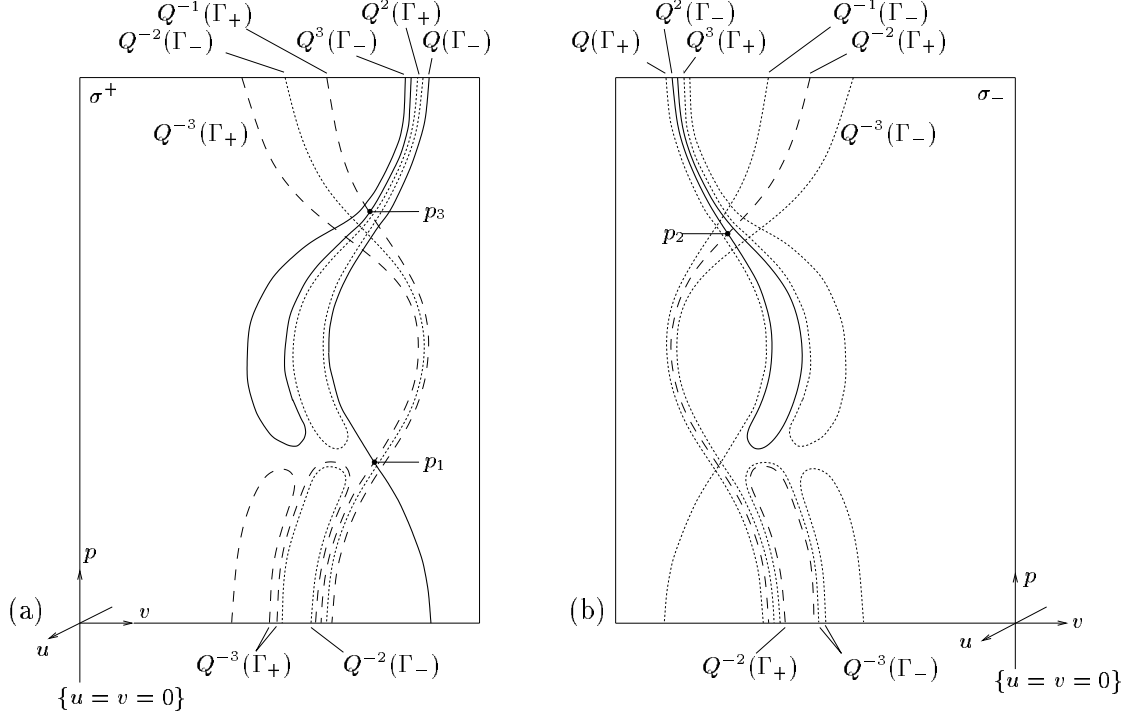


Figure 2: (a) The Poincaré section σ^+ . The solid curves are intersections $W^u(\Gamma_-) \cap \sigma^+$, the dashed curves are intersections $W^s(\Gamma_+) \cap \sigma^+$, and dotted curves represent both $W^u(\Gamma_+) \cap \sigma^+$ and $W^s(\Gamma_-) \cap \sigma^+$. (b) The Poincaré section σ^- . The solid curves again represent $W^u(\Gamma_-)$, the dashed curves represent $W^s(\Gamma_+) \cap \sigma^-$, and dotted curves are in $W^u(\Gamma_+) \cap \sigma^-$ or $W^s(\Gamma_-) \cap \sigma^-$.

close to $Q^{-1}(\Gamma_-)$ and $O(1)$ lower with respect to p . By combining the information for points $O(\varepsilon)$ away from and points exponentially close to $Q^{-1}(\Gamma_-)$, we find a difference between the upper and the lower part of $Q^{-1}(\Gamma_-)$: the preimages of the upper part form a branch $Q^{-2}(\Gamma_+)$ extending from $p = +\infty$ ($O(\varepsilon)$ close to $Q^{-1}(\Gamma_-)$) to $p = -\infty$ (exponentially close to $Q^{-1}(\Gamma_-)$), while the preimages of the lower part form a tongue $Q^{-2}(\Gamma_+)$ with two ends that extend to $p = -\infty$. This is illustrated by Figure 2(b).

Now applying Q_- to $Q^2(\Gamma_-)$ we find a tongue $Q^3(\Gamma_-) \subset \sigma^+$ that is an $O(\varepsilon)$ shift of $Q^2(\Gamma_-)$ mapped onto σ_+ . The preimage of $Q^{-2}(\Gamma_+)$ consists of three disjoint parts $Q^{-3}(\Gamma_+)$ in σ^+ . Both $Q^3(\Gamma_-)$ and $Q^{-3}(\Gamma_+)$ are indicated in Figure 2(a).

This procedure can be repeated to obtain further intersections of $W^u(\Gamma_-)$ and $W^s(\Gamma_+)$ with σ^+ and σ^- . Analogously (pre)images of the curves $Q(\Gamma_+)$ and $Q^{-1}(\Gamma_-)$, clarifying the structure of $W^u(\Gamma_+)$ and $W^s(\Gamma_-)$, can be found. By the identities (3.5), (3.6) $Q^n(\Gamma_+) = I_-(Q^n(\Gamma_-))$ for n even, $Q^n(\Gamma_+) = I_+(Q^n(\Gamma_-))$ for n odd, and $Q^{-m}(\Gamma_-) = I_+^{-1}(Q^{-m}(\Gamma_+))$ for m even, $Q^{-m}(\Gamma_-) = I_-^{-1}(Q^{-m}(\Gamma_+))$ for m odd.

It is shown in [8] that the procedure can be continued to obtain curves $Q^{\pm n}(\Gamma_{\pm})$ for all $n = O(|\log \varepsilon|)$; the same can be proved here.

Figure 2 shows part of the structure we described above. All tongues $Q^n(\Gamma_{\pm}) \subset \sigma^+$ (and $Q^n(\Gamma_{\pm}) \subset \sigma^-$) are disjoint, and so are the tongues and branches $Q^{-m}(\Gamma_{\pm}) \subset \sigma^+$

(and $Q^{-m}(\Gamma_{\pm}) \subset \sigma^{-}$), since (un)stable manifolds cannot self-intersect. The $Q^n(\Gamma_{\pm})$ curves are just single tongues, but each $Q^{-m}(\Gamma_{\pm})$ consists of m distinct curves. One of these is a *branch* ‘paralleling’ $Q^{-1}(\Gamma_+)$, the one closest to the $\{u = v = 0\}$ -axis is the *root tongue* of $Q^{-m}(\Gamma_+)$, and the others are all parts of *halos* surrounding the root tongues $Q^{-k}(\Gamma_+) \subset W^s(\Gamma_+)$ for $1 < k < m$ odd and $Q^{-k}(\Gamma_-) \subset W^s(\Gamma_-)$ for $1 < k < m$ even.

The different tongues in $W^u(\Gamma_{\pm})$ are ordered with increasing n , and tongues $Q^n(\Gamma_-)$ and $Q^{n+1}(\Gamma_+)$ alternate. This is indicated by alternating solid and dotted tongues in the figure. The root tongues in $W^s(\Gamma_{\pm})$ are ordered and alternate in the same way. The tongues in the halos of $Q^{-m}(\Gamma_{\pm})$ also alternate, in the sense that there is a tongue $Q^{-l-1}(\Gamma_-)$ around each tongue $Q^{-l}(\Gamma_+)$ or vice versa.

Note that the flow in p direction is always upwards for forward time, so the slow and the fast fields cooperate; see our discussion in §2.2. This implies that the ‘tip’ of the forward image of a tongue will have larger p -coordinate than the tip of the tongue itself, and that the tongues $Q^n(\Gamma_{\pm})$ cannot intersect the tongues $Q^{-m}(\Gamma_{\pm})$. Thus the only intersection points $Q^n(\Gamma_{\pm}) \cap Q^{-m}(\Gamma_{\pm})$ are the ones we already found: branches $Q^{-m}(\Gamma_p m)$ intersect $Q(\Gamma_{\pm})$ near $p = p^-$ and $p = p^+$, and tongues $Q^n(\Gamma_{\pm})$ intersect branches $Q^{-m}(\Gamma_{\pm})$ near $p = p^+$.

Whether the behaviour is cooperating or counteracting can only be measured by the p -direction here, since the flow is three-dimensional in this case.

Remark 3.5 The structures of $W^u(\Gamma_{\pm}) \cap \sigma^+$, $W^s(\Gamma_{\pm}) \cap \sigma^+$ are very similar to the structures of the stable and unstable manifolds in the Poincaré section in [8], where homoclinic connections to one slow manifold are considered.

Proof of Theorem 3.2. An n -jump orbit is, by construction, homoclinic to either Γ_+ or Γ_- for n even, and heteroclinic for n odd. For n odd, the orbits must either cross σ^- in $Q(\Gamma_+) \cap Q^{-n}(\Gamma_-)$ or cross σ^+ in $Q(\Gamma_-) \cap Q^{-n}(\Gamma_+)$.

By the above arguments we know that both intersections consist of exactly two points, one near $p = p^+$ and the other near $p = p^-$. Thus there are four n -jump heteroclinic orbits for each odd n . The application of Q_+ to σ^+ or Q_- to σ^- shows that all points are mapped to corresponding intersections $Q^k(\Gamma_{\pm}) \cap Q^{-l}(\Gamma_{\mp})$ with $n = k + l - 1$ that all lie in the neighbourhood of $p = p^+$. Hence the result is proved for n odd. The case n even follows analogously. \square

In Figure 3 two 3-jump orbits are sketched. They pass σ^+ , σ^- and σ^+ respectively through points $Q(\Gamma_-) \cap Q^{-3}(\Gamma_+)$, $Q^2(\Gamma_-) \cap Q^{-2}(\Gamma_+)$ and $Q^3(\Gamma_-) \cap Q^{-1}(\Gamma_+)$.

We have already defined the primary bifurcation value $c^*(a, q) = a + \tilde{c}(q)$. Since we consider the fixed hyperplane $\{q = \frac{1}{c}\}$ here, it is more convenient so view a as the bifurcation parameter that depends on c , and use $a^*(c)$ rather than $c^*(a)$ for the primary bifurcation near $c - a = 0$. (The c we chose also determines the parameter $q = \frac{1}{c}$ in $c^*(a, q)$.) As a increases from $a^*(c)$, the new multiple-jump homoclinic and heteroclinic orbits are created in a sequence of secondary bifurcations a_n^* depending on c .

Property 3.6 For fixed $c \neq 0$ the bifurcation values $a_n^*(c)$ satisfy:

1. For a^* there is exactly one heteroclinic orbit from Γ_- to Γ_+ and one from Γ_+ to Γ_- . For $a < a^*$, $W^u(\Gamma_{\pm}) \cap W^s(\Gamma_{\pm}) = \emptyset$, and for $a > a^*$ there are two one-jump heteroclinic orbits in both directions.

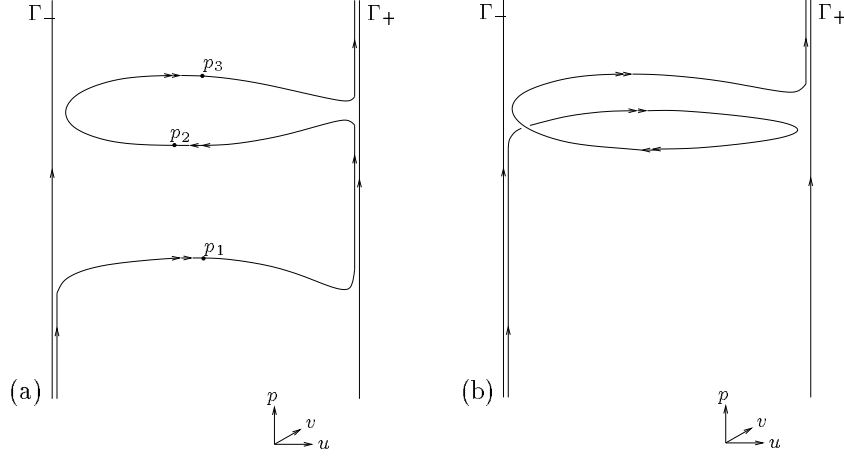


Figure 3: (a) One 3-jump orbit in $W^u(\Gamma_-) \cap W^s(\Gamma_+)$, connecting Γ_- with Γ_+ . The corresponding intersections p_i , $i = 1, 2, 3$, with σ^+ and σ^- are also indicated in Figure 2. (b) The second 3-jump orbit in $W^u(\Gamma_-) \cap W^s(\Gamma_+)$.

2. For each c fixed there exists a sequence of values a_n^* with $a_{n+1}^* > a_n^*$ for $n > 1$ and $a_2^* > a^*$, at which a pair of n -jump orbits asymptotic to Γ_- for $\xi \rightarrow -\infty$ and a pair asymptotic to Γ_+ for $\xi \rightarrow -\infty$ are created in a saddle-node bifurcation.

For n odd, two pairs of intersection points $Q^{-n}(\Gamma_{\pm}) \cap Q(\Gamma_{\mp})$ exist for $a > a_n^*$, while they do not exist for $a < a_n^*$. These intersections correspond to heteroclinic connections $\Gamma_{\mp} \rightarrow \Gamma_{\pm}$.

For n even, there are two intersections $Q^{-n}(\Gamma_-) \cap Q(\Gamma_-)$ and two intersection points $Q^{-n}(\Gamma_+) \cap Q(\Gamma_+)$ for $a > a_n^*$, that do not exist for $a < a_n^*$. These intersections correspond to homoclinic orbits connecting Γ_{\pm} to themselves.

3. For $n = O(1)$, $a_{n+1}^* - a_n^* = O(\varepsilon^2(\log \varepsilon)^2)$, and the bifurcations satisfy the iterative process $a_{n+1}^* = a_n^* + O(a_n^*)$ for all n .

We neither prove these properties here, nor explain the bifurcation mechanisms. A complete description of these mechanisms is given in section 4 of [8], and the proof of Property 3.6 follows immediately from the proofs there.

Remark 3.7 The symmetry (3.4) transforms the set $\{W^u(\Gamma_+) \cup W^s(\Gamma_+) \cup W^u(\Gamma_-) \cup W^s(\Gamma_-)\} \cap \sigma^+$ into $\{W^u(\Gamma_-) \cup W^s(\Gamma_-) \cup W^u(\Gamma_+) \cup W^s(\Gamma_+)\} \cap \sigma^-$. When this symmetry is broken, the Melnikov functions that measure the splitting in respectively Σ_- and Σ_+ are no longer identical. This means for instance that for certain values of a , c heteroclinic connections $\Gamma_- \rightarrow \Gamma_+$ can exist while there are no $\Gamma_+ \rightarrow \Gamma_-$ connections, or vice versa. Likewise, the higher order connections are not created in exactly the same bifurcations.

The symmetry is not essential for finding all homoclinic and heteroclinic orbits in this system however, but more bookkeeping is needed when it is broken.

We now consider the full system again. Define $\sigma_{\bar{q}}^{\pm} \stackrel{\text{def}}{=} \Sigma^{\pm} \cap \{q = \bar{q}\}$ and consider an arbitrary plane $\sigma_{\bar{q}}^{\pm}$ with $\bar{q} \geq 0$, $\bar{q} \neq \frac{1}{c}$. By the Melnikov calculations $Q(\mathcal{M}_-)$ and

$Q^{-1}(\mathcal{M}_+)$ intersect $\sigma_{\bar{q}}^{\pm}$ in curves that intersect each other at $p = p^{\pm}(\bar{q})$. We define these curves as $Q(\mathcal{M}_-)_{\bar{q}}$ and $Q^{-1}(\mathcal{M}_+)_{\bar{q}}$. Curves $Q(\mathcal{M}_+)_{\bar{q}}$ and $Q^{-1}(\mathcal{M}_-)_{\bar{q}}$ in $\sigma_{\bar{q}}^-$ are defined similarly.

To study the action of Q_+ on $Q(\mathcal{M}_-)_{\bar{q}}$, we can apply Corollary 2.4 and Lemma 2.6 as in the three-dimensional sub-system, however, $\Delta Q \neq 0$ now. $\Delta Q(p, \bar{q}, E) = O(\varepsilon)$ as long as $\bar{q} = O(1)$, $\Delta E(p, \bar{q}, E)$ differs only $O(\varepsilon^2)$ from $\Delta E(p, \frac{1}{c}, E)$, and $\Delta P(p, \bar{q}, E)$ differs $O(\varepsilon)$ from and has the same sign as $\Delta P(p, \frac{1}{c}, E)$; see (3.9), (3.10) and (3.11), and recall that we took $c, \bar{q} > 0$. We apply this to prove the following theorem:

Theorem 3.8 *For $c > 0$, $c - a = O(1) > 0$, and arbitrary n , there exist two families $\gamma_h^i(\xi; q, n)$, $i = 1, 2$, with $\lim_{\xi \rightarrow -\infty} d(\gamma_h^i(\xi), \mathcal{M}_-) = 0$ and two families $\tilde{\gamma}_h^i(\xi; q, n)$, $i = 1, 2$, with $\lim_{\xi \rightarrow -\infty} d(\tilde{\gamma}_h^i(\xi), \mathcal{M}_+) = 0$, of n -jump homoclinic or heteroclinic orbits as solutions of (3.2). All families are parameterized by q .*

We prove the theorem for $q \geq 0$ here, the proof for $q < 0$ will follow in § 3.3.

Proof. Take $c > 0$, $c - a = O(1) > 0$, so that the structure of $Q^{\pm 1}(\mathcal{M}_{\pm})$ is as in Figure 1. Consider $Q(\mathcal{M}_-)_{\bar{q}}$ with $\bar{q} \geq 0$. We divide the curve $Q(\mathcal{M}_-)_{\bar{q}}$ into three parts again (two pieces exponentially close to $Q^{-1}(\mathcal{M}_+)$, and one $O(\varepsilon)$ away from $Q^{-1}(\mathcal{M}_+)$), and apply Q_{\pm} repeatedly.

The images of points x on $Q(\mathcal{M}_-)_{\bar{q}}$ with $d(x, Q^{-1}(\mathcal{M}_+)) = O(\varepsilon)$ form a curve $O(\varepsilon)$ close to $Q(\mathcal{M}_+)_{\bar{q}}$, which does not lie in $\sigma_{\bar{q}}^-$, but $O(\varepsilon)$ close to this plane (since $\Delta Q = O(\varepsilon) \neq 0$). Q_+ works on points $x \in Q(\mathcal{M}_-)_{\bar{q}}$ exponentially close to $Q^{-1}(\mathcal{M}_+)$ like it does on similar points in $Q(\Gamma_-)$: the orbits through these points x come exponentially close to \mathcal{M}_+ , where $\dot{p}|_{\mathcal{M}_+} = O(\varepsilon) > 0$ stretches the orbits $O(1)$ upwards with respect to p , and the images $Q_+(x)$ lie exponentially close to $Q(\mathcal{M}_+)$. But now, since $\Delta Q = O(\varepsilon) \neq 0$, the q -coordinate may also change with an $O(1)$ amount. On \mathcal{M}_+ all orbits are asymptotic to $q = \frac{1}{c}$ as $\xi \rightarrow \infty$ by (3.3), so orbits that follow \mathcal{M}_+ for $O(\frac{1}{\varepsilon})$ time tend to $q = \frac{1}{c}$ before they leave \mathcal{M}_+ again. Hence the images of points on $Q(\mathcal{M}_-)_{\bar{q}}$, exponentially close to $p = p^+$, form a curve that lies exponentially close to $Q(\mathcal{M}_+)$, and is asymptotic to $Q(\Gamma_+)$. The points on $Q(\mathcal{M}_-)_{\bar{q}}$, exponentially close to $p = p^-$, form a similar curve. When we connect these curves to the part $O(\varepsilon)$ close to $Q(\mathcal{M}_+)_{\bar{q}}$, we obtain a continuous curve $Q_+(Q(\mathcal{M}_-)_{\bar{q}})$. Its projection onto $\sigma_{\bar{q}}^-$ (or every other plane σ_q^-) is a tongue like $Q^2(\Gamma_-)$, and the collection of all curves $Q_+(Q(\mathcal{M}_-)_{\bar{q}})$, $\bar{q} > 0$, forms a two-dimensional ‘gully’ $Q^2(\mathcal{M}_-)$ in Σ_- . Since both ends of this gully extend to $p = +\infty$, it intersects $Q^{-1}(\mathcal{M}_-)$ in two curves close to $p = p^+$. this establishes the existence of the two one-parameter families of 2-jump orbits homoclinic to \mathcal{M}_- .

The next image, $Q^3(\mathcal{M}_-)$, can thus be found combining information about points exponentially close to these intersections (Lemma 2.6) and about points $O(\varepsilon)$ away from $Q^{-1}(\mathcal{M}_-)$ (Corollary 2.4). It turns out to be a two-dimensional gully in Σ_+ , that is an $O(\varepsilon)$ shift of $Q^2(\mathcal{M}_-)$ mapped onto Σ_+ , with ends that lie exponentially close to $Q(\mathcal{M}_-)$ and are asymptotic to $Q(\Gamma_-)$.

Repeating these arguments, we find a collection of two-dimensional gullies $Q^n(\mathcal{M}_-)$ that lie in Σ_+ for n odd, in Σ_- for n even. Each of them intersects either $Q^{-1}(\mathcal{M}_+)$ or $Q^{-1}(\mathcal{M}_-)$ in two curves near $p = p^+$. These intersection curves represent families of n -jump homoclinic or heteroclinic orbits, parameterized by the base-points q , where $q \geq 0$. They connect \mathcal{M}_- with itself (n even) or \mathcal{M}_+ (n odd). Symmetric counterparts $Q^n(\mathcal{M}_+)$

and corresponding families of n -jump orbits are found by applying I_+ or I_- to $Q^n(\mathcal{M}_-)$. This completes the proof for $q \geq 0$. \square

Note, that we proved the existence by only determining the structure of $W^u(\mathcal{M}_\pm)$ and intersections $Q^{-1}(\mathcal{M}_\pm) \cap Q^n(\mathcal{M}_\pm)$. For $0 \leq k < n$ the $(n - k)$ th jump of each orbit whose existence we proved crosses Σ_+ or Σ_- in a point in $Q^{n-k}(\mathcal{M}_\pm) \cap Q^{-1-k}(\mathcal{M}_\pm)$. If we also know the global structure of $W^s(\mathcal{M}_\pm)$, or in other words all preimages $Q^{-n}(\mathcal{M}_\pm)$ of $Q^{-1}(\mathcal{M}_\pm)$, we can locate all these intersections and the corresponding jumps, as we did in Theorem 3.2 for the sub-system. We will not go into the details of this structure, but it can be found by arguments similar to those in the present and the next sections.

The main reason why the arguments used to find $W^u(\Gamma_\pm)$ also apply to $W^u(\mathcal{M}_\pm)|_{q \geq 0}$ is that \dot{p} has a definite sign that does not change along orbits in this region (in forward time). For this reason it is clear, that each section $Q^{-1}(\mathcal{M}_+)|_{\bar{q}}$ only contains orbits that travel upwards with respect to p , which basically gives the gully-structure. However, the sign of \dot{p} changes along forward orbits with initial points in $q < 0$. This is the reason that we did not address $q < 0$ in the proof of Theorem 3.2 yet. In the next section we address the effects of a changing \dot{p} (or \dot{q}) sign along orbits, corresponding to certain counteracting effects.

Remark 3.9 Not only the structure of the full two-dimensional gullies $Q^n(\mathcal{M}_\pm)$ in $q > 0$ (and of $Q^{-m}(\mathcal{M}_\pm)$ in $q > \frac{1}{c}$ – we did not show this) is reminiscent of the structure of $Q^n(\Gamma_\pm)$ and $Q^{-m}(\Gamma_\pm)$, but also the bifurcation mechanism by which they are created is similar to the mechanism in the three-dimensional sub-system.

This means, that the fourth dimension does not cause significant new behaviour in this region, but merely forms an extension of the three-dimensional problem: the phase space for $q \geq \frac{1}{c}$ is isomorphic to the product of the phase space restricted to $\{q = \frac{1}{c}\}$ and $\mathbf{R}_{\geq 1/c}$.

In the next subsection and in section 4 we will encounter more complicated behaviour, caused by significant influence of the fourth dimension on the global structure.

3.3 Influence of the fourth dimension: counteracting effects

As mentioned above, we did not consider orbits with initial conditions (and base points) in sections $\sigma_{\bar{q}}^\pm$ with $\bar{q} < 0$ so far, because the sign of \dot{p} changes (in forward time) on such orbits. As long as $d(x_0, Q^{-1}(\mathcal{M}_+)) = O(\varepsilon)$ for a point $x_0 = (0, v_0, p_0, q_0) \in Q(\mathcal{M}_-)$ inside $Q^{-1}(\mathcal{M}_+)$, its image $Q_+(x_0)$ has coordinates $(u_1, v_1, p_1, q_1) = (0, -v_0 + O(\varepsilon), p_0 + O(\varepsilon|\log \varepsilon|), q_0 + O(\varepsilon|\log \varepsilon|))$ by (3.10), (3.11), (A.16) in the Appendix and Lemma 2.5. Whether $q_0 > 0$ or $q_0 < 0$ does not make a significant difference here, although it does determine whether $q_1 > q_0$, $p_1 > p_0$, or vice versa. If x_0 lies exponentially close to $Q^{-1}(\mathcal{M}_+)$ however, Lemma 2.6 imposes that the forward orbit through x_0 will follow \mathcal{M}_+ for an $O(1)$ distance. If in this case $q_0 \geq 0$, then the p -coordinate will always increase with an $O(1)$ amount, which we exploited in the previous subsection. If $q_0 < 0$, then the p -coordinate will decrease as long as q stays negative, but might increase afterwards, depending on the time the orbit spends exponentially close to \mathcal{M}_+ and on the orbit in \mathcal{M}_\pm it follows. In Figure 4(a) we schematically show some orbits with different initial

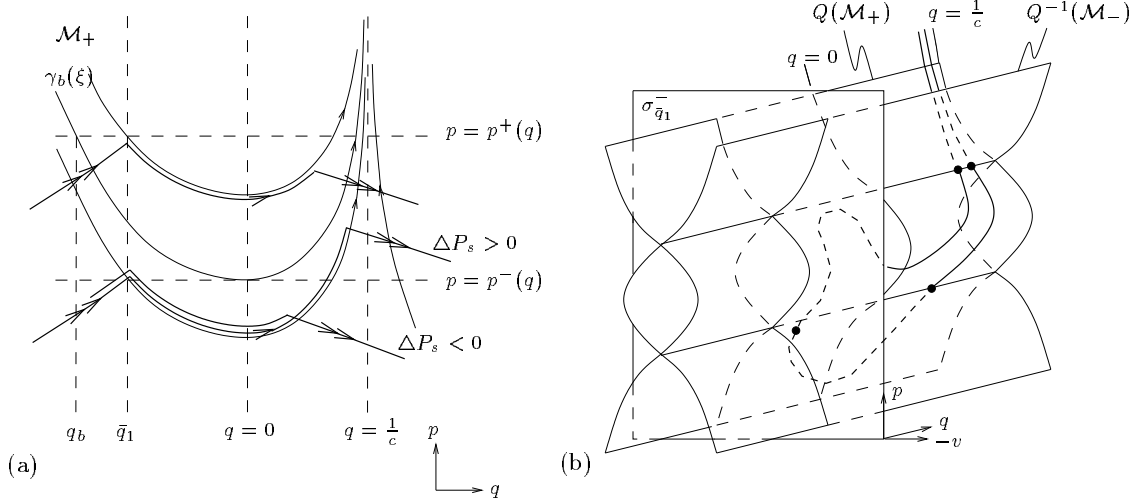


Figure 4: $b = 0$, $c > 0$, $c - a = O(1) > 0$. (a) Passage exponentially close to \mathcal{M}_+ of orbits through $Q(\mathcal{M}_-)_{\bar{q}_1}$ with $q_b'' < \bar{q}_1 < q_b'$. The value $q_b = q_b'' + O(\varepsilon)$ and the corresponding orbit $\gamma_b(\xi)$ are indicated. (b) The image curve $Q_+(Q(\mathcal{M}_-)_{\bar{q}_1})$ in Σ_- .

points $x_0 \in Q(\mathcal{M}_-)$ exponentially close to $Q^{-1}(\mathcal{M}_+)$ (and thus to $p = p^\pm(\bar{q}_1)$) and $q_0 = \bar{q}_1 < 0$. They exhibit different types of qualitative behaviour. Since the points x_0 lie in $Q(\mathcal{M}_-) \subset W^u(\mathcal{M}_-)$ and are exponentially close to $Q^{-1}(\mathcal{M}_+)$, the orbits are exponentially close to $W^s(\mathcal{M}_+) \cap W^u(\mathcal{M}_-)$ and enter the neighbourhood of \mathcal{M}_+ exponentially close to $p^+(\bar{q}_1)$ or $p^-(\bar{q}_1)$.

To prove existence of rich classes of n -jump homoclinic or heteroclinic orbits, we introduce the boundary value $q_b < 0$ as follows. Let $c > 0$, $c - a > 0$, and let $\gamma_b(\xi)$ be the (boundary) orbit in \mathcal{M}_+ with $\gamma_b(0) = (1, 0, p^-, 0)$. Then there exists a value $\Xi < 0$ such that $\gamma_b(\Xi) = (1, 0, p^+, q(\Xi))$. We define $q_b = q(\Xi) < 0$. Note, that this value can be defined for all $c - a > 0$, and that it satisfies

$$(3.12) \quad -q_b - \frac{1}{c} \log(1 - cq_b) = 2c\sqrt{c - a}$$

by the slow flow (3.3). A similar value \tilde{q}_b can be defined on \mathcal{M}_- . Since the flows on \mathcal{M}_+ and \mathcal{M}_- are equal for (3.2), $q_b = \tilde{q}_b$. The value q_b and the corresponding orbit $\gamma_b(\xi)$ are indicated in Figure 4(a).

Theorem 3.10 *Consider (3.2) with $c > 0$, $c - a = O(1) > 0$ and $n \geq 1$. There exist bifurcation values $q_b' = 0 + O(\varepsilon)$ and $q_b'' = q_b + O(\varepsilon)$, such that for all $q_b'' < q < q_b'$ there are $2n$ families $\gamma_h^i(\xi; q, n)$ with $\lim_{\xi \rightarrow -\infty} d(\gamma_h^i(\xi), \mathcal{M}_-) = 0$, and $2n$ families $\tilde{\gamma}_h^i(\xi; q, n)$, satisfying $\lim_{\xi \rightarrow -\infty} d(\tilde{\gamma}_h^i(\xi), \mathcal{M}_+) = 0$, of n -jump homoclinic or heteroclinic orbits. Moreover, for $q < q_b''$ there exist $4n - 2$ families $\gamma_h^i(\xi; q, n)$ and $4n - 2$ families $\tilde{\gamma}_h^i(\xi; q, n)$ with the same properties. For $q > q_b'$ only two such families $\gamma_h^i(\xi; q, n)$ and $\tilde{\gamma}_h^i(\xi; q, n)$ exist. The index i in the notation numbers the different families.*

The families with $q < 0$ mentioned in Theorem 3.8 are precisely the two families in Theorem 3.10 that exist for all q . We first investigate the images of curves $Q(\mathcal{M}_-)_q$ with $\bar{q} < 0$ and then prove Theorem 3.10.

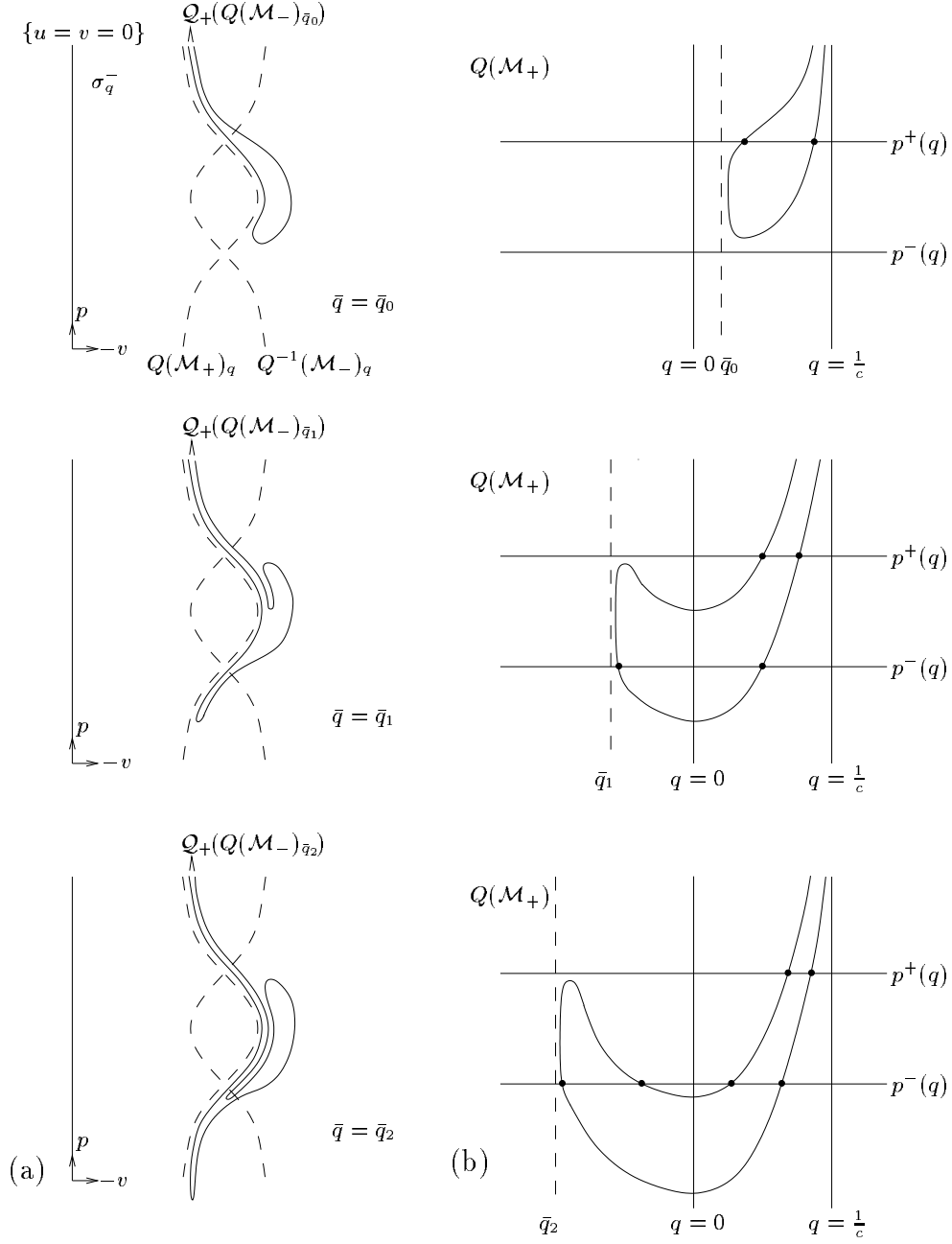


Figure 5: (a) Images $Q_+(Q(\mathcal{M}_-)_q)$ for $\bar{q} = \bar{q}_{0,1,2}$, projected onto a plane $\sigma_q^- \subset \Sigma_-$. $Q(\mathcal{M}_+)_q = I_+(Q(\mathcal{M}_-)_q)$ and $Q^{-1}(\mathcal{M}_-)_q = I_-^{-1}(Q^{-1}(\mathcal{M}_+)_q)$ are drawn to clarify the picture. (b) Images $Q_+(Q(\mathcal{M}_-)_q)$, projected onto $Q(\mathcal{M}_+) \subset \Sigma_-$ for $\bar{q} = \bar{q}_{0,1,2}$.

Consider the curve $Q(\mathcal{M}_-)_\bar{q}$ in a section $\sigma_{\bar{q}}^\pm$ with $\bar{q} < 0$. Following the above reasoning for $\bar{q} > 0$ we find that \mathcal{Q}_+ maps the part of $Q(\mathcal{M}_-)_\bar{q}$ that is $O(\varepsilon)$ away from $Q^{-1}(\mathcal{M}_+)$ to a curve inside and $O(\varepsilon)$ away from $Q(\mathcal{M}_+)$. Points $x_1 \in Q(\mathcal{M}_-)_\bar{q}$ exponentially close to $Q^{-1}(\mathcal{M}_+)$ lie on orbits that follow the flow on \mathcal{M}_+ for an $O(1)$ distance. Depending on the length of the trajectory close to \mathcal{M}_+ , \dot{p} can stay negative, or may change sign. In the former case $\Delta P_s < 0$ clearly, but in the latter case the final increment of the p -coordinate may be larger than the first decrement, which makes a positive ΔP_s possible. The images of the points x_1 form two tongues exponentially close to $Q(\mathcal{M}_+)$ as in the three pictures in Figure 5(a), the upper consisting of images of points close to $p = p^+(\bar{q})$ and the lower of images of points near $p = p^-(\bar{q})$. These tongues both extend to $p = +\infty$ and are asymptotic to $q = \frac{1}{\varepsilon}$ by the slow flow (3.3). We call them ‘thin’ tongues, since they are only exponentially thin with respect to the v -coordinate, but note that they are $O(1)$ wide with respect to the q -coordinate. Combining this with the information about points $x_0 \in Q(\mathcal{M}_-)$ with $d(x_0, Q^{-1}(\mathcal{M}_+)) = O(\varepsilon)$, we find a curve $\mathcal{Q}_+(Q(\mathcal{M}_-)_\bar{q}) \in \Sigma_-$ that is connected by continuity, and intersects $Q^{-1}(\mathcal{M}_-)$ in at least two points close to $p = p^-(q)$, corresponding to two 2-jump homoclinic orbits to \mathcal{M}_- . See Figure 4(b).

The orbits through $Q(\mathcal{M}_-)_\bar{q}$ that follow \mathcal{M}_+ exactly until $\dot{p} = 0$ have the largest negative ΔP_s and correspond to the minima in p of the curve $\mathcal{Q}_+(Q(\mathcal{M}_-)_\bar{q})$. Let these orbits be $\gamma_{\min}^+(\xi; \bar{q})$ and $\gamma_{\min}^-(\xi; \bar{q})$ respectively. The more negative \bar{q} is, the deeper the thin tongues become, because orbits through (p^\pm, \bar{q}) stay longer in the $\dot{p} < 0$ régime. First the lower little tongue will intersect $Q^{-1}(\mathcal{M}_-)$ close to $p = p^-(0)$, yielding two extra 2-jump orbits. This happens in a bifurcation $\bar{q} = q'_b$, which is defined such that $\gamma_{\min}^-(\xi; q'_b)$ follows the orbit in \mathcal{M}_+ that is tangent to $\{p = p^-\}$. Since this tangency in \mathcal{M}_+ occurs at $q = 0$, q'_b obviously satisfies $q'_b = 0 + O(\varepsilon)$. At $q = q'_b$ two additional 2-jump orbits bifurcate. For even more negative \bar{q} the upper little tongue will also intersect $Q^{-1}(\mathcal{M}_-)$ close to $p = p^-$. Here the bifurcation is given by $\bar{q} = q''_b = q_b + O(\varepsilon)$ since the orbit $\gamma_b(\xi; q_b)$ in \mathcal{M}_+ is tangent to $\{p = p^-\}$. In Figure 5 projections of the image-tongues for $\bar{q}_2 < q''_b < \bar{q}_1 < q'_b < \bar{q}_0$ are shown.

These arguments prove that the counteracting behaviour along orbits possibly leads to two or four additional families of 2-jump homoclinic orbits to \mathcal{M}_- . The first pair bifurcates at $q = q'_b$ and the second at $q = q''_b$. By the symmetry, such families of orbits homoclinic to \mathcal{M}_+ exist also. This proves Theorem 3.10 for $n = 2$.

We now construct further images for $\bar{q} < q'_b$. The images for $\bar{q} > q'_b$ are analogous to those for $q > 0$.

Note, that $\mathcal{Q}_+(Q(\mathcal{M}_-)_\bar{q})$, $\bar{q} < q'_b$, consists of either two or three disjoint parts inside $Q^{-1}(\mathcal{M}_+)$, depending on the relative position of \bar{q} and q''_b . In Figure 6 these parts are indicated by their boundary points, intersections with $Q^{-1}(\mathcal{M}_+)$ that are numbered 1 to 6. The intersections 1 and 4 correspond to orbits in the two families of Theorem 3.8. These intersections always exist. The intersections 2 and 3 correspond to the lower thin tongue, the intersections 5 and 6 to the upper. They exist when respectively $\bar{q} < q'_b$ and $\bar{q} < q''_b$. Hence for $q''_b < \bar{q} < q'_b$ the two disjoint parts inside $Q^{-1}(\mathcal{M}_+)$ are 1–2 and 3–4, and for $\bar{q} < q''_b$ the three disjoint parts are 1–2, 4–5, and 3–6. To map $\mathcal{Q}_+(Q(\mathcal{M}_-)_\bar{q})$ to $\mathcal{P}_+(Q(\mathcal{M}_-)_\bar{q})$ we consider these different parts of the curve $\mathcal{Q}_+(Q(\mathcal{M}_-)_\bar{q})$ separately (recall that $\mathcal{P}_+ = \mathcal{Q}_- \circ \mathcal{Q}_+$).

From the flow on \mathcal{M}_+ and in the fast field we know, that the parts to the left of

the minima of the thin tongues (with Figure 5(a) as reference picture) lie in the region $q > 0$, as illustrated by the projections in Figure 5(b). Hence $\dot{q} > 0$ on the further forward trajectories. Since these parts also lie exponentially close to $Q(\mathcal{M}_+)|_{0 < q < 1/c}$, repeated application of \mathcal{Q}_- and \mathcal{Q}_+ maps these parts exponentially close to the consecutive images of $Q(\mathcal{M}_+)|_{0 < q < 1/c}$. Therefore, the forward images of the parts 1–2 and 4–5 (the latter if it exists) form tongue-like curves $Q^n(Q(\mathcal{M}_-)|_{\bar{q}})$, $n > 1$, around the gullies $Q^n(\mathcal{M}_+)|_{0 < q < 1/c}$, and thus each of these curves intersects $Q^{-1}(\mathcal{M}_\pm)$ twice, giving rise to two $(n+1)$ -jump orbits. See Figure 6, where the images 1'–2' and 4'–5' in $Q^2(Q(\mathcal{M}_-)|_{\bar{q}}) = \mathcal{P}_+(Q(\mathcal{M}_-)|_{\bar{q}})$ are sketched. Note that every original curve intersects $Q^{-1}(\mathcal{M}_-)$ two times, and that all their further image curves intersect either $Q^{-1}(\mathcal{M}_+)$ or $Q^{-1}(\mathcal{M}_-)$ twice as well: every intersection point $Q^{-1}(\mathcal{M}_\pm) \cap Q^n(Q(\mathcal{M}_-)|_{\bar{q}})$ with q -coordinate $q > 0$ yields an intersection point $Q^{-1}(\mathcal{M}_\mp) \cap Q^{n+1}(Q(\mathcal{M}_-)|_{\bar{q}})$.

If the upper thin tongue does not extend to $p = p^-(q)$, then the part between its minimum and the point 4 has images that lie along $Q^n(\mathcal{M}_+)|_{0 < q < 1/c}$, but do not form full tongues around them. They intersect $Q^{-1}(\mathcal{M}_\pm)$ only once. See Figure 6(a).

However, the parts of $\mathcal{Q}_+(Q(\mathcal{M}_-)|_{\bar{q}})$ to the right of the minima of the thin tongues (with respect to Figure 5(a)) still lie in the $q < 0$ region, so again counteracting effects can occur along the forward trajectories of these parts. The largest part in $q < 0$ inside $Q^{-1}(\mathcal{M}_-)$ is $O(\varepsilon)$ away from $Q^{-1}(\mathcal{M}_-)$ and is thus just mapped over an $O(\varepsilon)$ distance by \mathcal{Q}_- (and $O(\varepsilon|\log \varepsilon|)$ with respect to p and q). Its image is simply a copy of the original curve. This is clearly illustrated by the image of 3–6 in Figure 6(b): the largest part of the tongue-like curve 3–6 is mapped to a similar large tongue-like part contained in 3'–6' in $\mathcal{P}_+(Q(\mathcal{M}_-)|_{\bar{q}})$. The parts of $\mathcal{Q}_+(Q(\mathcal{M}_-)|_{\bar{q}})$ that are exponentially close to the intersection points 3 and 6 contain orbits that follow \mathcal{M}_- for an $O(1)$ distance. By the same arguments as above, the images of these points form two thin tongues in $\mathcal{P}_+(Q(\mathcal{M}_-)|_{\bar{q}})$, exponentially close to $Q(\mathcal{M}_-)$ in Σ_+ . Both intersect $Q^{-1}(\mathcal{M}_+)$ in two points near $p = p^-$ and in one point close to $p = p^+$ as in Figure 6(b). For $\bar{q} > q_b''$, for which the intersection point 6 in $\mathcal{Q}_+(Q(\mathcal{M}_-)|_{\bar{q}})$ does not exist, only the points near 3 give rise to a thin tongue in $\mathcal{P}_+(Q(\mathcal{M}_-)|_{\bar{q}})$, see Figure 6(a).

Similar arguments can be applied to find further images. To resume, every intersection point $\mathcal{Q}_+(Q(\mathcal{M}_-)|_{\bar{q}}) \cap Q^{-1}(\mathcal{M}_-)$ (or later, every point $Q^n(Q(\mathcal{M}_-)|_{\bar{q}}) \cap Q^{-1}(\mathcal{M}_\pm)$) in the region $q < 0$ gives rise to a thin tongue exponentially close to $Q(\mathcal{M}_\pm)$ that intersects $Q^{-1}(\mathcal{M}_\pm)$ two times near $p = p^-$ and one time near $p = p^+$. One of the resulting intersection points near $p = p^-$ still lies in the region $q < 0$, the other (and the point close to $p = p^+$) in the region $q > 0$.

Proof of Theorem 3.10. We determine the number of n -jump homoclinic or heteroclinic orbits that exist by induction. We consider a curve $Q(\mathcal{M}_-)|_{\bar{q}} \subset \Sigma_+$, and apply \mathcal{Q}_\pm repeatedly to obtain image curves. Label the number of intersection points that these curves make with $Q^{-1}(\mathcal{M}_\pm)$ and that correspond to n -jump orbits by C_n . Among these intersection points there are A_n with q -coordinate $q > 0$, and B_n with q -coordinate $q < 0$. By the above observations these numbers satisfy the recursive relations

$$\begin{aligned} A_{n+1} &= A_n + 2B_n, \\ B_{n+1} &= B_n. \end{aligned}$$

For $q_b'' < \bar{q} < q_b'$ the initial conditions are $A_2 = 3$, $B_2 = 1$, leading to $A_{n+1} = A_n + 2$ and

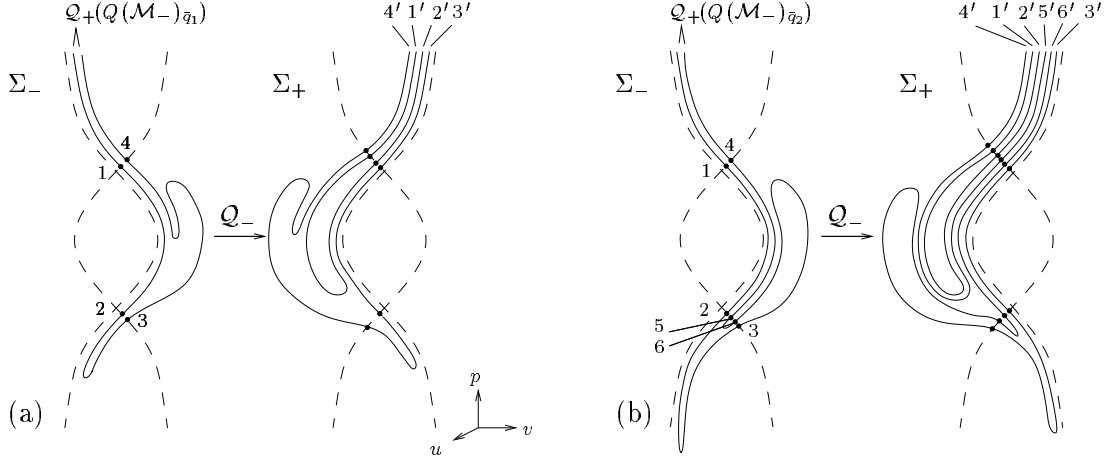


Figure 6: Images $\mathcal{P}_+(Q(\mathcal{M}_-)\bar{q}) \subset \Sigma_+$ projected onto a plane $\sigma_q^+ \subset \Sigma_+$ and the relation between the parts $i-j$ of $\mathcal{Q}_+(Q(\mathcal{M}_-)\bar{q}) \subset \Sigma_-$ and their images $i'-j'$ in $\mathcal{P}_+(Q(\mathcal{M}_-)\bar{q})$. The dashed curves represent $Q^{\pm 1}(\mathcal{M}_{\pm})$. The orientation is the same in all figures. (a) $\bar{q} = \bar{q}_1$, $q_b'' < \bar{q}_1 < q_b'$; (b) $\bar{q} = \bar{q}_2$ with $\bar{q}_2 < q_b''$.

$C_n = 2n$. For $\bar{q} < q_b''$ we have initial conditions $A_2 = 4$, $B_2 = 2$, which yield $A_{n+1} = A_n + 4$ and $C_n = 4n - 2$. Clearly the two intersection points near $p = p^+$ with $q > 0$ always exist, these are element of the families of Theorem 3.8.

These numbers only represent the orbits through $Q(\mathcal{M}_-)\bar{q}$, which are asymptotic to \mathcal{M}_- as $\xi \rightarrow -\infty$. The symmetry (3.4) yields equal numbers of orbits that are asymptotic to \mathcal{M}_+ as $\xi \rightarrow -\infty$. \square

4 Coupled slow and fast flows: more counteracting effects

Although the example in the previous section might a priori have seemed rather trivial, we have seen that it exhibits very rich behaviour. The structures of the intersections of stable and unstable manifolds of \mathcal{M}_{\pm} will become yet more complicated when we choose different, less trivial and perhaps more realistic, functions G and K . In this section we extend the example with a coupling term in perturbation K . We choose a coupling that is quadratic in U , since such term preserves the symmetry (3.4). Since this symmetry is broken by linear or, in general, odd terms, the quadratic coupling is the simplest one in a sense. The example we take is

$$(4.1) \quad \begin{aligned} U_t &= U_{xx} - U^3 + U - \varepsilon U_x(P^2 + a), \\ P_t &= P_{xx} - \varepsilon^2(1 + b(U^2 - 1)), \end{aligned}$$

leading to the ODE

$$(4.2) \quad \begin{aligned} u_{\xi} &= v, \\ v_{\xi} &= u^3 - u + \varepsilon v(p^2 + a - c), \\ p_{\xi} &= \varepsilon q, \\ q_{\xi} &= \varepsilon(1 + b(u^2 - 1) - cq). \end{aligned}$$

Note that we write $1 + b(U^2 - 1)$ instead of $bU^2 + \tilde{b}$. In this form the equation is a clear perturbation of (3.1), and the additional perturbation term is equal to zero on the slow manifolds and non-zero in the fast field. We will exploit this in the study of more counteracting effects in this example.

Clearly, the extra term does not change the behaviour of the fast field, so the Melnikov calculations do not change. However, the integral ΔQ gets an extra term and becomes

$$(4.3) \quad \Delta Q(E, p, q) = \varepsilon(1 - cq)T_0(E) - \varepsilon b\tilde{T}_2(E) + O(\varepsilon^2).$$

Together with (3.9) and (3.10) this yields the following conditions on periodic orbits in (4.2) with $c - a > 0$, $b \neq 0$:

$$p = \pm\sqrt{c - a} + O(\varepsilon), \quad q = 0 + O(\varepsilon), \quad \text{and} \quad \mathcal{T}(E) = \frac{1}{b} + O(\varepsilon),$$

with

$$\mathcal{T}(E) \stackrel{\text{def}}{=} \frac{\tilde{T}_2(E)}{T_0(E)}.$$

In the regions $q < \frac{1}{c}$ and $q > \frac{1}{c}$ the flows on the slow manifolds \mathcal{M}_\pm do not change sign with respect to q . Therefore, within each region the slow contributions ΔQ_s , as defined in § 2.2, always have the same sign. The average flow $\Delta Q(E, p, q)$ in the fast field might however change sign within the regions and be cooperating or counteracting. The bound between the cooperating and the counteracting régime with respect to the flow in q -direction is given by $\Delta Q(E, p, q) = 0$, $q \neq \frac{1}{c}$, so at leading order by

$$\mathcal{T}(E) \stackrel{\text{def}}{=} \frac{\tilde{T}_2(E)}{T_0(E)} = \frac{1 - cq}{b}, \quad q \neq \frac{1}{c}.$$

In the Appendix it is shown that $0 \leq \mathcal{T}(E) \leq 1$ and $\frac{d}{dE}\mathcal{T} < 0$ for $0 < E < \frac{1}{4}$ (note that $f(p) \equiv 1$ here), so for each $q \neq \frac{1}{c}$ such that $\frac{1 - cq}{b} \in [0, 1]$ there is exactly one E such that $\Delta Q(E, p, q) = 0$. For $q = 0$, this condition coincides with the existence condition for periodic orbits. This means that for each $b \in [0, 1]$ there is a unique E such that $\Delta Q(E, p, 0) = 0$ and two periodic orbits exist, one $O(\varepsilon)$ close to $(p, q) = (p^+, 0)$ and one $O(\varepsilon)$ close to $(p, q) = (p^-, 0)$.

For $b < 0$ there are no solutions of $\Delta Q(E, p, q) = 0$ in the region $1 - cq > 0$, and for $b > 0$ such solutions do not exist in the region $1 - cq < 0$. Thus the system is always cooperating in one of these regions. From (4.4) below one can even conclude that the slow and fast fields cooperate for all $b < 1 - cq$ in the region $1 - cq > 0$, and for all $b > 1 - cq$ in the region $1 - cq < 0$. Considering the limiting behaviour of $T_0(E)$ and $\tilde{T}_2(E)$ in the neighbourhoods of $E = 0$ and $E = \frac{1}{4}$ (see (A.1), (A.16) and (A.17) in the Appendix) we have

$$(4.4) \quad \lim_{E \downarrow 0} \Delta Q(E, p, q) = \varepsilon(1 - cq - b)2\pi + O(\varepsilon^2),$$

$$(4.5) \quad \Delta Q(\tfrac{1}{4} - \eta, p, q) = \varepsilon\sqrt{2}(1 - cq)|\log \eta| - \varepsilon b 4\sqrt{2} + \text{h.o.t. when } 0 < \eta \ll \tfrac{1}{4},$$

and we conclude that a small counteracting region near $\{u = 0, v = 0\}$ (where $E = 0$) comes up when b crosses $b = 1 - cq$. As b increases (or decreases, depending on the sign of c), the counteracting régime within the $q = O(1)$ region grows until eventually, for $b = O(|\log \varepsilon|)$ and positive enough, it includes the neighbourhoods of $W^u(\mathcal{M}_\pm)$ and $W^s(\mathcal{M}_\pm)$ (take $\eta \sim \varepsilon$). We will show that this counteracting behaviour near $W^{u,s}(\mathcal{M}_\pm)$ yields new families of homoclinic and heteroclinic orbits, while the families that exist for $b = 0$ stay intact.

In the previous section we studied images $Q^n(Q(\mathcal{M}_-)_\bar{q})$ of curves $Q(\mathcal{M}_-)_\bar{q} \subset \sigma_{\bar{q}}^+$ for $b = 0$. We recall that for $\bar{q} < q_b''$ both the upper and the lower intersection point $Q(\mathcal{M}_-)_\bar{q} \cap Q^{-1}(\mathcal{M}_+) \in \Sigma_+$ (respectively near $p^+(\bar{q})$ and $p^-(\bar{q})$) induce two intersections $Q_-(Q(\mathcal{M}_-)_\bar{q}) \in \Sigma_-$ near $p^-(q)$ and one such intersection near $p^+(q)$. For $q_b'' < \bar{q} < q_b'$, the upper intersection point only induces the one intersection near $p^+(q)$, while the lower still also yields two intersections near $p^-(q)$. See Figure 5. This induction also holds for higher order intersections in these regions *if they exist*.

Higher order intersections in the region $q < 0$ arise by the following mechanism. Consider an orbit $\gamma(\xi)$ that comes exponentially close to \mathcal{M}_+ and follows the flow on \mathcal{M}_+ , until it leaves the neighbourhood of \mathcal{M}_+ with q -coordinate $0 < q_0 < \frac{1}{c}$. Assume that it passes Σ_- at $\xi = \xi_1$ in $\gamma(\xi_1) = (0, v_1, p_1, q_1)$ inside $Q^{-1}(\mathcal{M}_-)$, and hence enters the neighbourhood of \mathcal{M}_- after spending $O(1)$ time in the fast field. Since $\gamma(\xi)$ is inside and exponentially close to $W^u(\mathcal{M}_+)_{\text{loc}}$ at $\xi = \xi_1$, it satisfies $E = \frac{1}{4} - \eta$ with $\eta = O(\varepsilon) > 0$, and the change in the q -coordinate during the time in the fast field is

$$\frac{1}{2} \triangle Q(\frac{1}{4} - \eta, p_1, q_1) = \frac{1}{2}[\varepsilon\sqrt{2}(1 - cq_1)|\log \eta| - \varepsilon b 4\sqrt{2}] + \text{h.o.t.}$$

We recall that $\triangle Q$ measures the average change of q during a full circuit through the fast field, so by the symmetry the change during the jump from \mathcal{M}_+ to \mathcal{M}_- is given by $\frac{1}{2} \triangle Q$. This expression is negative at leading order if $b > \frac{1}{4}(1 - cq_1)|\log \eta| > 0$. Thus, if $b = O(|\log \varepsilon|)$ and large enough the orbit $\gamma(\xi)$ touches down on \mathcal{M}_- with $q_2 = q_0 + \frac{1}{2} \triangle Q(\frac{1}{4} - \eta, p_1, q_1) < q_0$ and $q_2 < 0$ is possible for $q_0 = O(\varepsilon|\log \varepsilon|)$.

We will use these observations to prove the occurrence of additional homoclinic saddle-node bifurcations for $b > 0$. As in section 6 of [8], the mechanisms behind these counteracting bifurcations are rather complicated, and iterative processes create more and more different ‘types’ of n -jump homoclinic and heteroclinic orbits. We do not attempt to describe every single process and bifurcation in detail, but rather prove one general property.

Property 4.1 *Consider (4.2) with fixed $c > 0$ such that $c - a > 0$. As b increases to $b = O(|\log \varepsilon|)$ a small region around $q = 0$ arises, where homoclinic saddle-node bifurcations occur by which new families of n -jump homoclinic and heteroclinic orbits appear. The families that already existed for $b = 0$ stay intact. As b increases further, more and more n -jump orbits are created.*

Proof. We apply Q_- to map a curve $Q(\mathcal{M}_-)_\bar{q} \subset \Sigma_-$ with $\bar{q} < q_b' \approx 0$ to Σ_+ , and vary b from $b = 0$ to $b = O(|\log \varepsilon|) > 0$. For $b = 0$ the proof of Theorem 3.10 guarantees the existence of at least three intersection points $Q_-(Q(\mathcal{M}_-)_\bar{q}) \cap Q^{-1}(\mathcal{M}_+)$ with $q > 0$ in Σ_+ , as illustrated by Figure 5(b). If $\bar{q} < q_b'$ and $|\bar{q} - q_b'| = O(\varepsilon|\log \varepsilon|)$, or $\bar{q} < q_b''$ and

$|\bar{q} - q_b''| = O(\varepsilon|\log \varepsilon|)$, then at least one of these intersection points lies $O(\varepsilon|\log \varepsilon|)$ close to $q = 0$.

As above, the symmetry yields that the fast field contributes to the change in the q -coordinates induced by mapping from Σ_- to Σ_+ with $\frac{1}{2} \Delta Q|_{b=0} = \varepsilon \frac{1}{2} \sqrt{2}(1 - cq)|\log \eta| + \text{h.o.t.}$ with $q \approx 0$. If we let b increase, this change will become $\frac{1}{2} \Delta Q|_{b>0} = \varepsilon \frac{1}{2} \sqrt{2}(1 - cq_1)|\log \eta| - \varepsilon b 2\sqrt{2} + \text{h.o.t.} < \frac{1}{2} \Delta Q|_{b=0}$. Since the changes in the integrals E and p are not influenced by b , the increment of b only translates the image curve $\mathcal{Q}_-(Q(\mathcal{M}_-)_\bar{q})$ parallel to the q -axis over a distance $-\varepsilon b 2\sqrt{2}$. Hence all intersection points $\mathcal{Q}_-(Q(\mathcal{M}_-)_\bar{q}) \cap Q^{-1}(\mathcal{M}_+)$, and thus the families of 2-jump orbits described in Theorem 3.10, will stay for increasing b .

However, if $\mathcal{Q}_-(Q(\mathcal{M}_-)_\bar{q})|_{b=0}$ contained intersection points with small $q > 0$ as described in the last paragraph, these intersection points can be translated to $q < 0$ for large enough b . This yields the existence of one or more additional higher order intersections (here $\mathcal{Q}_-(Q(\mathcal{M}_-)_\bar{q}) \cap Q^{-1}(\mathcal{M}_+)$, corresponding to 2-jump orbits) in the region $\{q < 0\}$. Such intersection points induce three, instead of one, 3-jump orbits in the next iteration. The recursive relation in the proof of Theorem 3.10 now immediately implies additional n -jump orbits with $n \geq 3$ as well. Moreover, among the new intersection points there are points with small $q > 0$ again, so the above arguments can be applied to prove the existence of even more additional n -jump orbits. All these orbits are asymptotic to \mathcal{M}_- as $\xi \rightarrow -\infty$.

If b increases, the region that will be translated from $q > 0$ to $q < 0$ is enlarged. Therefore this mechanism applies to a wider range of curves $Q(\mathcal{M}_-)_\bar{q} \subset \Sigma_-$ (with \bar{q} farther from q_b' or q_b'') and the families of new n -jump homoclinic or heteroclinic orbits become larger.

All arguments can also be applied to curves in $Q(\mathcal{M}_+)$, and doing so the same result is obtained for orbits that are asymptotic to \mathcal{M}_+ as $\xi \rightarrow -\infty$. \square

Remark 4.2 A naive extension of these ideas would be to take $\Delta Q < 2(q_b - \frac{1}{c})$, which would guarantee that all intersection points induced by the flow near $\mathcal{M}_-|_{q < 1/c}$, including those through orbits that jump off \mathcal{M}_- close to $q = \frac{1}{c}$, are carried to the $q < q_b''$ region near \mathcal{M}_+ . This would result in three $(n+1)$ -jump orbits induced by every n -jump orbit in $\{q < \frac{1}{c}\}$, which would result in $2 \cdot 3^n$ n -jump orbits.

However, b needs to be of order $O(\frac{1}{\varepsilon})$ to obtain $\Delta Q < 2(q_b - \frac{1}{c})$. Rescaling $b = \frac{B}{\varepsilon}$ gives the ODE system

$$\begin{aligned} u_\xi &= v, \\ v_\xi &= u^3 - u + \varepsilon v(p^2 + a - c), \\ p_\xi &= \varepsilon q, \\ q_\xi &= B(u^2 - 1) + \varepsilon(1 - cq). \end{aligned}$$

It still possesses slow manifolds given by $u = \pm 1, v = 0$, but these manifolds no longer satisfy Fenichel's condition of normal hyperbolicity. Therefore the geometric singular perturbation theory is no longer applicable for $b = O(\frac{1}{\varepsilon})$.

The above calculations show that for $b < 0$ the slow and fast flows in the region $1 - cq < 0$ counteract. However, the sign of \dot{p} still does not change along orbits, which prevents any bifurcation of additional n -jump orbits in this region.

For $b = O(|\log \varepsilon|)$ and b negative enough, ΔQ can become positive enough to carry orbits from the $q < 0$ to the $q > 0$ region, and let part of the n -jump families of Theorem 3.10 disappear. In a sense, this mechanism is the inverse of the mechanism in the proof of Property 4.1.

5 Numerical simulations

In this section we study the behaviour of (1.1) by numerical simulations. The goals of the numerical simulations are to find out whether the n -jump orbits constructed in the previous sections can be observed as travelling front solutions of (3.1), and to see which speed is selected as ‘most stable’ speed, that is, with which speed the observed solutions travel. The numerical code should select one specific speed, since, given any value of a , the analysis in sections 3 and 4 guarantees existence of n -jump homoclinic and heteroclinic orbits that travel with any speed bigger than some critical speed $c_n^*(a)$.

5.1 The numerical code

We used a so-called moving-grid code to integrate (4.1). This code by Blom and Zegeling is described in detail in [4], and applied intensively to reaction-diffusion systems in for instance [10, 6, 22]. The code is designed to numerically solve systems of time-dependent PDEs in one space dimension having solutions with steep gradients in space and time, so the homoclinic and heteroclinic solutions constructed in the previous sections can perfectly be studied with this code. In order to do numerical simulations the space variable x has to be restricted to a bounded interval. To ensure that the boundaries of this interval do not (essentially) influence the dynamics this interval must be large enough. For the simulations presented here we fixed the length of the interval on $x \in [0, 200]$. We investigated intervals of different lengths and chose the interval so large that enlarging did not influence the front-type behaviour of solutions with only a small number of fronts.

The space variable x is scaled to \tilde{x} such that the simulations take place on the interval $\tilde{x} \in [0, 1]$. For the U -variable, that jumps from $U = -1$ to $U = +1$ and vice versa, we both took homogeneous Neumann boundary-conditions

$$\frac{\partial U}{\partial \tilde{x}}(\tilde{x} = 0, t) = \frac{\partial U}{\partial \tilde{x}}(\tilde{x} = 1, t) = 0$$

and Dirichlet boundary-conditions

$$U(\tilde{x} = 0, t) = \pm 1, \quad U(\tilde{x} = 1, t) = \pm 1,$$

depending on the type of solution we searched. The different choices did not influence the dynamics of the solutions. The initial conditions were adapted to the kind of solutions of our interest. Both block functions with the desired number of fronts and functions composed of arctan-shaped fronts were used as initial conditions for U . The different functions with the same number of initial fronts all gave the same result, which indicates that the observed multi-front waves are attracting.

If $b = 0$ and the velocity $c \neq 0$ of a travelling pattern is known, the function P can be solved explicitly from (3.2):

$$p(\xi) = \frac{\varepsilon \xi}{c} - C_1(c)e^{-\varepsilon c \xi} + C_2(c),$$

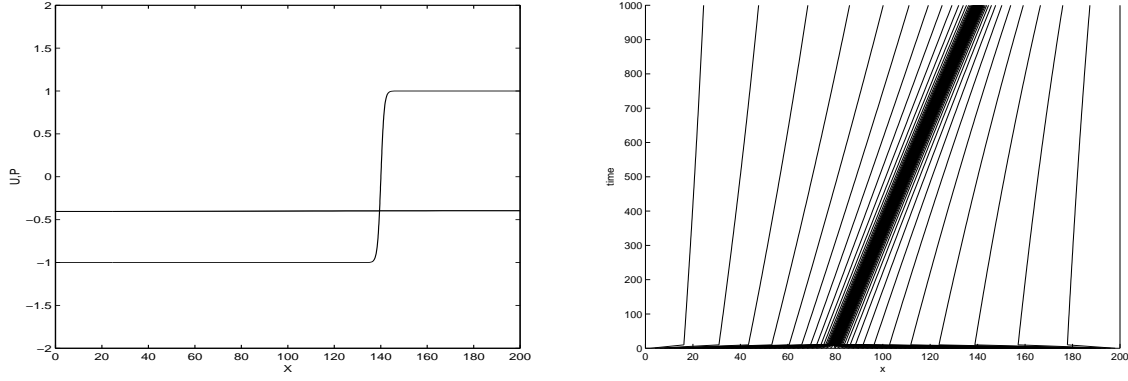


Figure 7: Travelling one-front heteroclinic orbit observed in a numerical simulation of (4.1) with $\varepsilon = 0.02$, $a = 3$ and $b = 0$ at time $t = 500$. The right picture shows positions of the grid points as functions of time for the same parameters. At any time instant the densest part of the grid corresponds to the front.

where $C_1(c)$ and $C_2(c)$ are constants depending on c . This expression indicates that Dirichlet boundary conditions for P are not suitable. We therefore simply took

$$(5.1) \quad P(\tilde{x}, 0) = \text{const.} \quad \text{or} \quad P(\tilde{x}, 0) = C\tilde{x} + D$$

and matched this with homogeneous Neumann boundary conditions

$$(5.2) \quad \frac{\partial P}{\partial \tilde{x}}(\tilde{x} = 0, t) = \frac{\partial P}{\partial \tilde{x}}(\tilde{x} = 1, t) = 0.$$

5.2 Simulations and observations

Independent of the initial condition for P , our simulations suggested that the velocity of the selected U -solution satisfies $c \approx a$. Therefore we put $C = \frac{2\varepsilon}{a}$ (and $D = 0$) together with $P(0, 0) = -\frac{2}{a}$ and $P(1, 0) = \frac{2\varepsilon}{a}$ in (5.1), or $P \equiv 0$ if $\frac{\varepsilon}{a}$ was very small. We investigated solutions with 1-4 initial fronts and different values ε , a and b and running times T . For the simulations with 1,2 fronts 100 moving grid points were sufficient, for more fronts we used 200 grid points.

A representative example with one front is plotted in Figure 7. As initial condition we took $U(x, 0) = \frac{2}{\pi} \arctan(x - 80)$ and $P(x, 0)$ as above with $a = 3$, $\varepsilon = 0.02$. The front clearly moves with a positive speed, that approximately satisfies $\varepsilon c = \Delta x / \Delta t \approx 60/1000 = 0.06$. Since $\varepsilon = 0.02$ this corresponds to $c \approx 3 = a$.

The second example shows a solution with three fronts for $a = -4$. Initially the fronts lay at $x = 90$, $x = 115$ and $x = 130$, but they immediately moved to respectively $x \approx 93$, $x \approx 115$ and $x \approx 133$ as one can see from the right picture in Figure 8. In simulations with different initial conditions the fronts analogously moved to a configuration that likely corresponds to a solution of (4.1). After this initial adjustment all three fronts moved with about the same speed -0.04 , since the dense parts of the grid are parallel (up to the current precision). Since $\varepsilon = 0.01$ this corresponds to $c \approx -4 = a$.

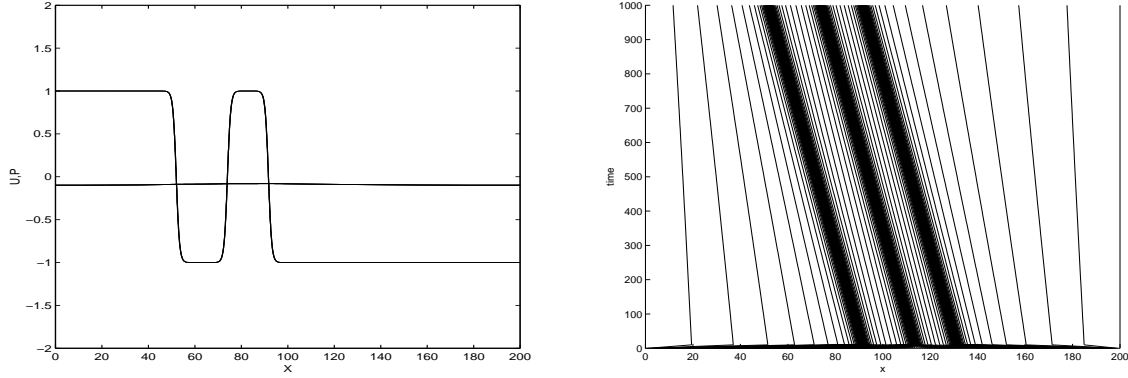


Figure 8: Travelling 3-front heteroclinic orbit observed in a numerical simulation of (4.1) with $\varepsilon = 0.01$, $a = -4$ and $b = 2$ at time $t = 500$. The right picture shows positions of the grid points as functions of time for the same parameters.

From the analysis in the previous sections we know that n -jump orbits exist whenever $c - a = O(1)$. For the sub-system with $P_\xi = \varepsilon q = \frac{\varepsilon}{c}$ the information is more detailed: for all $n = O(|\log \varepsilon|)$ there are n -jump orbits that travel with speed $c \geq c_n^*(a)$. From Property 3.6 we know that $c_n^*(a) = O(\varepsilon^2(\log \varepsilon)^2)$ for all $n = O(1)$, or, in other words, that $c_n^*(a) = a + O(\varepsilon^2(\log \varepsilon)^2)$.

The simulations here clearly show that the solution to which the integration converges travels with a speed that satisfies $c \approx a$. This suggests that the solution that is selected by the numerical code satisfies $c = c_n^*(a)$, in other words, the simulations strongly suggest that for every n the solution with the lowest possible speed is the ‘most stable’ one. Such a selection of the bifurcation speed as the most stable speed also occurs in other systems. As an example we mention the well-known Kolmogorov-Petrovsky-Piscounov (KPP) equation $U_t = U_{xx} + U - U^2$ ($x \in \mathbf{R}$, $t > 0$), where for any $c \geq 2$ travelling waves with velocity c exist, and the wave with velocity $c = 2$ is generally selected as most stable one; see §5.4 of [14].

6 Discussion

The work in this paper mainly consisted of an extension of the methods of [9, 8, 13] to four-dimensional systems. The most important conclusion is that the global behaviour of systems as (1.7) is still largely determined by the flow on the slow manifold. With the extra dimension we find that even the simplest equations (3.2) exhibit very complicated behaviour.

Fenichel’s persistence theory can only be applied to compact subsets of the unperturbed normally hyperbolic manifold \mathcal{M}_0 . The two examples considered in this paper generate a (slow) flow on \mathcal{M}_ε that will leave any bounded $O(1)$ region for $|\xi| \geq \frac{1}{\varepsilon}$. Moreover, p and q will eventually become so large that (1.6) can no longer be considered as a perturbation problem. This is not a special feature of the four-dimensional problem. The work by Ai [1] on the three-dimensional problem proposed in [8] for instance shows that n -pulse orbits

‘homoclinic’ to a slow manifold do not remain close to that manifold for $|t| \geq \frac{1}{\varepsilon}$. To avoid problems with perturbations in (1.6) that become $\gg 1$ one must either compactify \mathcal{M} (see [8, 13]) or ‘repair’ the perturbations for p, q large, such that they remain small (see [9]). By the structure of the originating PDE neither of these approaches can be applied to the p_ξ, q_ξ equations in (1.6). However, since the region $p, q = O(1)$ is the only relevant part of the phase space in which one can find intersections of the manifolds $W^{u,s}(\mathcal{M}_\pm)$, we do not really need to adapt the flow as sketched above. Homoclinic or heteroclinic orbits we find may not remain close to one of the slow manifolds for $|\xi| \geq \frac{1}{\varepsilon}$, but this would not influence the ‘jumping structure’ of the orbit.

By the numerical simulations we are sure that at least some of the orbits we construct are observed in the dynamics of the PDE for long periods of time. Moreover, the problems on the slow manifold for $p, q \gg 1$ are implicitly caused by the simplicity of the examples considered in this paper. Less ‘trivial’ examples will not have only unbounded solutions on the slow manifold \mathcal{M}_ε . On the contrary, a slow flow with critical points is certainly more realistic. In such a realistic situation the homoclinic and heteroclinic solutions will become connections between these critical points (on the slow manifolds) instead of only connections between the manifolds. As a consequence, the solutions will remain in a bounded region of the phase space and none of the ‘problems’ sketched above will arise.

Nevertheless, in this paper we decided not to consider a more realistic example with critical points on \mathcal{M}_\pm , but to focus on two simpler examples and take the possible ‘undesired behaviour’ for $|\xi| \gg 1$ for granted. Certainly, more realistic examples can also be studied by the methods presented in this paper, but their phase structure will be harder to unravel.

Both the Gray-Scott model for auto-catalysis [10] and a large family of generalized Gierer-Meinhardt-like systems [7] have been studied with methods that are in essence the same as the ones presented here. These systems generate slow manifolds that do have a critical point. However, their phase structure is significantly less complicated than the structures here, since there is a reversibility symmetry owing to the absence of ‘convective’ terms. The proof of the existence of n -pulse homoclinic orbits in [10, 7] is largely based on this symmetry and is, for that reason, relatively simple compared to the proof of Theorem 3.8 here. On the other hand, the reversibility symmetry in these models gives the phase space so much structure that one cannot expect to have phenomena as exciting as the homoclinic explosions and subshift dynamics of [9] and [13]. Our analysis of two trivial examples of equation (1.6), an equation that includes ‘convective’ effects, has shown that such phenomena may be observed in systems of this type.

We stress once more, that the methods presented in this paper are applicable to a very general class of four-dimensional systems of ODEs with two slow and two fast variables and a heteroclinic or homoclinic manifold in the fast limit. Hence, the methods presented here are of a more general interest than only for the type of equations derived for PDEs as (1.1). Although we only worked out the details of two explicit examples it follows from these examples that the general idea of the methods developed in [9, 8, 13] also applies to many four-dimensional singularly perturbed systems.

We cannot claim anything about the stability of the numerically observed orbits. The simulations strongly suggest that at least some of the multi-front orbits can be stable, or

meta-stable, as solutions to the PDE. Recently, a number of new methods to study the stability of multi-pulse solutions to (singularly perturbed) systems of reaction-diffusion equations were developed; see [23, 6, 7]. These methods might be useful for the stability analysis of the patterns constructed in this paper.

References

- [1] S. Ai. *Multi-pulse Orbits for a Singularly Perturbed Nearly-integrable System*. Ph. D. thesis, University of Pittsburgh, 1999.
- [2] J. Alexander, R. A. Gardner, and C. K. R. T. Jones. A topological invariant arising in the stability of travelling waves. *J. reine angew. Math.*, **410**:167–212, 1990.
- [3] D. Armbruster, J. Guckenheimer, and P. Holmes. Heteroclinic cycles and modulated travelling waves in systems with $O(2)$ symmetry. *Physica D*, **29**:257–282, 1988.
- [4] J. G. Blom and P. A. Zegelting. Algorithm 731: A moving-Grid Interface for Systems of One-Dimensional Time-Dependent Partial Differential Equations. *ACM Transactions in Math. Software*, **20**:194–214, 1994.
- [5] A. Doelman. Breaking the hidden symmetry in the Ginzburg-Landau equation. *Physica D*, **97**:398–428, 1996.
- [6] A. Doelman, R. A. Gardner, and T. J. Kaper. Stability analysis of singular patterns in the 1-D Gray-Scott model: a matched asymptotic approach. *Physica D*, **122**:1–36, 1998.
- [7] A. Doelman, R. A. Gardner, and T. J. Kaper. Large stable pulse solutions in reaction diffusion equations. To appear in *Indiana Univ. Math. J.*, 2000.
- [8] A. Doelman and G. M. Hek. Homoclinic saddle-node bifurcations in singularly perturbed systems. *J. Dyn. Diff. Eq.*, **12**(1):169–216, 2000.
- [9] A. Doelman and P. Holmes. Homoclinic explosions and implosions. *Phil. Trans. R. Soc. Lond. A* , **354**:845–893, 1996.
- [10] A. Doelman, T. J. Kaper, and P. Zegelting. Pattern formation in the one-dimensional Gray-Scott model. *Nonlinearity*, **10**:523–563, 1997.
- [11] N. Fenichel. Geometric singular perturbation theory for ordinary differential equations. *J. Diff. Eq.*, **31**:53–98, 1979.
- [12] T. Gallay. Periodic patterns and traveling fronts for the Ginzburg-Landau equation. In A. Mielke and K. Kirchgässner, editors, *Proceedings of the IUTAM/ISSIM Symposium Structure and Dynamics of Nonlinear waves in Fluids* , pages 230–238. World Scientific, 1995. Adv. Series in Nonlin. Dyn., Vol. **7**.
- [13] G. M. Hek, A. Doelman, and P. J. Holmes. Homoclinic Saddle-Node Bifurcations and Subshifts in a Three-Dimensional Flow. *Arch. Rat. Mech. Anal.*, **145**:291–329, 1998.

- [14] D. Henry. *Geometrical Theory of Semilinear Parabolic Equations*. Springer-Verlag, New-York, 1981. Lecture Notes in Mathematics No. **840**.
- [15] C. K. R. T. Jones. Geometric Singular Perturbation Theory. In R. Johnson, editor, *Dynamical Systems, Montecatini Terme*, Lecture Notes in Math. **1609**, pages 44–118. Springer-Verlag, Berlin, 1994.
- [16] C. K. R. T. Jones, T. J. Kaper, and N. Kopell. Tracking Invariant Manifolds up to Exponentially Small Errors. *SIAM J. Math. Anal.*, **27**(2):558–577, 1996.
- [17] C. K. R. T. Jones and N. Kopell. Tracking Invariant Manifolds with Differential Forms in Singularly Perturbed Systems. *J. Diff. Eq.* , **108**(1):64–88, 1994.
- [18] T. Kapitula and J. Rubin. Existence and stability of standing hole solutions to complex Ginzburg-Landau equations. *Nonlinearity*, **13**(1):77–112, 2000.
- [19] H. Kokubu, K. Mischaikow, and H. Oka. Existence of infinitely many connecting orbits in a singularly perturbed ordinary differential equation. *Nonlinearity*, **9**(5):1263–80, 1996.
- [20] J. D. Murray. *Mathematical Biology*. Springer-Verlag, New York, etc., 1989.
- [21] C. Robinson. Sustained resonance for a nonlinear system with slowly varying coefficients. *SIAM Math. An.* , **14**:847–860, 1983.
- [22] V. Rottschäfer and A. Doelman. On the transition from the Ginzburg-Landau equation to the extended Fisher-Kolmogorov equation. *Physica D*, **118**:261–292, 1998.
- [23] B. Sandstede. Stability of multiple-pulse solutions. *Trans. Amer. Math. Soc.*, **350**(2):429–472, 1998.
- [24] S. Wiggins. *Introduction to Applied Nonlinear Dynamical Systems and Chaos*. Springer-Verlag, New York etc., 1990.

A Appendix

We derive some useful properties of the complete elliptic integrals $T_i(E)$ defined in (3.7) and (3.8). By perturbation analysis around $E = 0$, $E = \frac{f(p)}{4}$ and integration of the limiting expressions we compute

$$(A.1) \quad \lim_{E \downarrow 0} T_0(E) = 2\pi, \quad \lim_{E \downarrow 0} T_2(E) = 0, \quad \lim_{E \uparrow \frac{1}{4}f(p)} T_0(E) = \infty \quad \text{and} \quad \lim_{E \uparrow \frac{1}{4}f(p)} \tilde{T}_2(E) = 4\sqrt{\frac{2}{f(p)}}.$$

In order to obtain information about limit behaviour of T_0 , \tilde{T}_2 and about \mathcal{T} we will express S_0 and $\frac{d}{dE}T_i$ in T_0 and T_2 (or \tilde{T}_2). Note that in all equations the i is an index. We first define

$$(A.2) \quad R_i(E) = \oint \frac{u^i}{(\frac{1}{2}f(p)u^4 - f(p)u^2 + 2E)^{\frac{3}{2}}} \text{ for } i \geq 0,$$

so

$$(A.3) \quad \frac{d}{dE}T_i(E) = -R_i(E).$$

and find the expression

$$(A.4) \quad T_i = 2ER_i - f(p)R_{i+2} + \frac{1}{2}f(p)R_{i+4} \text{ for } i \geq 0.$$

Furthermore, rewriting S_i yields

$$(A.5) \quad S_i = \oint \frac{u^i(\frac{1}{2}f(p)u^4 - f(p)u^2 + 2E)}{\sqrt{\frac{1}{2}f(p)u^4 - f(p)u^2 + 2E}} du = \frac{1}{2}f(p)T_{i+4} - f(p)T_{i+2} + 2ET_i \text{ for } i \geq 0.$$

Since the integral around a closed curve of any exact differential vanishes, we have

$$(A.6) \quad \begin{aligned} 0 &= \oint \frac{d}{du} \left(u^i \sqrt{\frac{1}{2}f(p)u^4 - f(p)u^2 + 2E} \right) du = iS_{i-1} - f(p)T_{i+1} + f(p)T_{i+3}, \\ &\text{for } i \geq 1, \\ 0 &= -T_1 + A_3. \end{aligned}$$

Combining (A.5) and (A.6) with $i = 0$ resp. $i = 1$ leads to the following expression for S_0 :

$$(A.7) \quad S_0(E) = (\frac{4}{3}E - \frac{1}{3}f(p))T_0(E) + \frac{1}{3}f(p)\tilde{T}_2(E).$$

We follow the methods presented in [3, 9] to derive $\frac{d}{dE}T_i(E)$. By the same arguments as those used to derive (A.6) we have

$$(A.8) \quad \begin{aligned} 0 &= \oint \frac{d}{du} \frac{u^i}{\sqrt{\frac{1}{2}f(p)u^4 - f(p)u^2 + 2E}} du = iT_{i-1} + f(p)R_{i+1} - f(p)R_{i+3}, \\ &\text{for } i \geq 1, \\ 0 &= R_1 - R_3. \end{aligned}$$

By taking $i = 0, 1, 2$ in (A.4), $i = 1, 2, 3$ in (A.6) and (A.8) we obtain a linear 7×7 system:

$$(A.9) \quad \begin{pmatrix} 2E & 0 & -f & 0 & \frac{f}{2} & 0 & 0 \\ 0 & 2E & 0 & -f & 0 & \frac{f}{2} & 0 \\ 0 & 0 & 2E & 0 & -f & 0 & \frac{f}{2} \\ 0 & 1 & 0 & -1 & 0 & 0 & 0 \\ 0 & 0 & -f & 0 & f & 0 & 0 \\ 0 & 0 & 0 & -f & 0 & f & 0 \\ 0 & 0 & 0 & 0 & -f & 0 & f \end{pmatrix} \begin{pmatrix} R_0 \\ R_1 \\ R_2 \\ R_3 \\ R_4 \\ R_5 \\ R_6 \end{pmatrix} = \begin{pmatrix} T_0 \\ T_1 \\ T_2 \\ 0 \\ T_0 \\ 2T_1 \\ 3T_2 \end{pmatrix}.$$

It follows immediately that $R_1 = R_3 = 0$, or, in other words, the expressions in the integrals R_1 and R_3 are exact differentials. We solve the system (A.9) to obtain expressions for R_0 and R_2 and hence for $\frac{d}{dE}T_i(E)$, $i = 0, 1, 2$ by (A.3): 28

$$(A.10) \quad \frac{dT_0}{dE} = \frac{f(p)T_2 - 4ET_0}{4E(-f(p) + 4E)}, \quad \frac{dT_1}{dE} = 0, \quad \frac{dT_2}{dE} = \frac{T_2 - T_0}{-f(p) + 4E} \text{ and } \frac{d\tilde{T}_2}{dE} = \frac{\tilde{T}_2 - T_0}{4E},$$

from which we derive

$$(A.11) \quad \frac{d}{dE}\mathcal{T} = \frac{f(p)\mathcal{T}^2 + (8E - 2f(p))\mathcal{T} + (f(p) - 4E)}{4E(-f(p) + 4E)}.$$

The discriminant of the polynomial $f(p)\mathcal{T}^2 + (8E - 2f(p))\mathcal{T} + (f(p) - 4E)$ is $16E(4E - f(p)) < 0$ for $0 < E < \frac{f(p)}{4}$, so it has no real roots and

$$(A.12) \quad \frac{d}{dE}\mathcal{T} < 0 \text{ for } 0 < E < \frac{f(p)}{4}.$$

Together with the limits $\lim_{E \downarrow 0} \mathcal{T}(E) = 1$ and $\lim_{E \uparrow \frac{f(p)}{4}} \mathcal{T}(E) = 0$ from (A.1) this yields $\mathcal{T}(E) \in [0, 1]$. To study the behaviour of \mathcal{T} in the neighbourhood of $E = \frac{f(p)}{4}$ we substitute $\mathcal{T}(\frac{f(p)}{4} - \eta) = \delta(\eta)$ with $\lim_{\eta \downarrow 0} \delta(\eta) = 0$ in (A.11) and find

$$(A.13) \quad \frac{d}{dE}\tilde{\mathcal{T}}(\frac{f(p)}{4} - \eta) = \frac{4\eta - 8\eta\delta + f(p)\delta^2}{-4\eta(f(p) - 4\eta)}.$$

We now show by a contradiction that $\delta(\eta) \gg \eta$ in the limit $\eta \downarrow 0$. Assume $\delta(\eta) = k\eta + \text{h.o.t.}$ Direct computation of $\frac{d}{dE}\mathcal{T}(\frac{f(p)}{4})$ from this assumption gives $\frac{d}{dE}\mathcal{T}(\frac{f(p)}{4}) = -k$. From (A.13) we obtain

$$\frac{d}{dE}\mathcal{T}(\frac{f(p)}{4}) = \lim_{\eta \downarrow 0} \frac{d}{dE}\mathcal{T}(\frac{f(p)}{4} - \eta) = \lim_{\eta \downarrow 0} \frac{4\eta + O(\eta^2)}{-4f(p)\eta + O(\eta^2)} = -\frac{1}{f(p)},$$

so $k = -\frac{1}{f(p)}$. Since we also have $\frac{d}{dE}\mathcal{T}(0) = -\frac{1}{f(p)}$ and \mathcal{T} is a continuous function, the curve $\mathcal{T}(E)$ should intersect $\mathcal{T} = 1 - \frac{4E}{f(p)}$, say in E^* . This would lead to

$$\frac{d}{dE}\mathcal{T}(E^*) = \frac{f(p)(1 - \frac{4E^*}{f(p)})^2 + (8E^* - 2f(p))(1 - \frac{4E^*}{f(p)}) + (f(p) - 4E^*)}{4E^*(-f(p) + 4E^*)} = -\frac{1}{f(p)}$$

which is impossible since $\frac{d}{dE}\mathcal{T}(E^*) < -\frac{4}{f(p)}$ is needed for an intersection with the line $\mathcal{T} = 1 - \frac{4E}{f(p)}$. Hence the assumption $\delta(\eta) = k\eta + \text{h.o.t.}$ must be rejected and $\delta \gg \eta$. Now δ can be derived from (A.13):

$$(A.14) \quad \frac{d}{d\eta}\delta(\eta) = -\frac{f(p)\delta^2}{4\eta} + \text{h.o.t.} \text{ and thus } \delta(\eta) = \frac{4}{f(p)|\log \eta|} + \text{h.o.t.}$$

Hence we end up with

$$(A.15) \quad \mathcal{T}\left(\frac{f(p)}{4} - \eta\right) = \frac{4}{f(p)|\log \eta|} + \text{h.o.t.}$$

and can conclude from this and (A.1) that for $0 < \eta \ll \frac{f(p)}{4}$:

$$(A.16) \quad T_0\left(\frac{f(p)}{4} - \eta\right) = \frac{\tilde{T}_2\left(\frac{f(p)}{4} - \eta\right)}{\mathcal{T}\left(\frac{f(p)}{4} - \eta\right)} = \sqrt{2f(p)|\log \eta|} + \text{h.o.t.}$$

Furthermore, by substituting (A.1) and (A.16) into (A.10) we find $\frac{d}{dE}\tilde{T}_2\left(\frac{f(p)}{4} - \eta\right) = O(|\log \eta|)$, which yields

$$(A.17) \quad \tilde{T}_2\left(\frac{f(p)}{4} - \eta\right) = 4\sqrt{\frac{2}{f(p)}} + O(\eta|\log \eta|).$$